PHYSICAL REVIEW D **108,** 014510 (2023)

Equation of state and speed of sound of (2 + 1)-flavor QCD in strangeness-neutral matter at nonvanishing net baryon-number density

D. Bollweg,[1,2] D. A. Clarke,[3,4] J. Goswami,[5] O. Kaczmarek,[3] F. Karsch,[3] Swagato Mukherjee,[1]
P. Petreczky,[1] C. Schmidt,[3] and Sipaz Sharma[3]

(HotQCD Collaboration)

[1]*Physics Department, Brookhaven National Laboratory, Upton, New York 11973, USA*
[2]*RIKEN-BNL Research Center, Brookhaven National Laboratory, Upton, New York 11973, USA*
[3]*Fakultät für Physik, Universität Bielefeld, D-33615 Bielefeld, Germany*
[4]*Department of Physics and Astronomy, University of Utah, Salt Lake City, Utah 84112, USA*
[5]*RIKEN Center for Computational Science, Kobe 650-0047, Japan*

(Received 27 December 2022; accepted 27 June 2023; published 19 July 2023)

We update results on the QCD equation of state in $(2+1)$-flavor QCD with nonzero conserved charge chemical potentials obtained from an eighth-order Taylor series. To construct bulk thermodynamic observables, we use continuum extrapolated results for the second and fourth order expansion coefficients of pressure, while using spline interpolated result based on high statistics $N_\tau = 8$ data for the sixth and eighth order expansion coefficients. We present results for basic bulk thermodynamic observables of strangeness-neutral strong-interaction matter, i.e., pressure, number densities, energy, and entropy density, and resum Taylor series results using Padé approximants. Furthermore, we calculate the speed of sound as well as the adiabatic compression factor of the strangeness-neutral matter on lines of constant entropy per net baryon number. We show that the equation of state $[P(n_B), \epsilon(n_B)]$ is already well described by the 4th-order Taylor series in almost the entire range of temperatures accessible with the beam energy scan in collider mode at the Relativistic Heavy Ion Collider.

DOI: 10.1103/PhysRevD.108.014510

I. INTRODUCTION

Fundamental properties of hot and dense matter controlled by the strong force are encoded in the equation of state (EoS). The EoS is sensitive to the change of degrees of freedom that dominate properties of strong-interaction matter at low temperatures and densities on the one hand and high temperature and densities on the other hand. It describes fluctuations of, e.g., energy and particle densities that signal the occurrence of phase transitions. The EoS finds application in the hydrodynamic modeling of hot and dense matter created in heavy ion collisions [1] and in constraining the "cosmic trajectory" of matter in the expanding early universe [2].

The EoS of strong-interaction matter is obtained from quantum chromodynamics (QCD) at finite temperature and non-zero values of the conserved charge chemical potentials. It is well studied at vanishing values of the chemical potentials [3–5]. For nonvanishing values of the chemical potentials that couple to net baryon number (μ_B), net electric charge (μ_Q), and net strangeness (μ_S), lattice QCD calculations have to face the well-known sign problem. Currently, this renders direct numerical calculations with nonzero, real-valued chemical potentials impossible. For this reason numerical calculations at nonzero (μ_B, μ_Q, μ_S) have been performed by either using Taylor expansions in terms of the chemical potentials, e.g., [6,7] or by performing numerical simulations at imaginary values of the chemical potential, [8,9]. Using the latter and analyzing results with various ansätze for an analytic continuation to real values of the chemical potential, the EoS of $(2+1)$-flavor QCD has been determined [10–12]. Following the Taylor expansion approach, results for the QCD EoS have been obtained from up to sixth-order expansions [13,14].

We extend here the Taylor expansion approach for the EoS in $(2+1)$-flavor QCD using recent high-statistics results for Taylor expansion coefficients up to eighth-order [15] in

---

(μ_B, μ_Q, μ_S). We will make use of the Padé-resummation of Taylor series discussed in [15] and determine direct Taylor series results as well as Padé-resummed approximants for pressure, net baryon-number, energy and entropy densities. Making use of our high-statistics data at temperatures in the vicinity of the pseudocritical temperature we will, for the first time, present contributions to higher-order derivatives of bulk thermodynamic observables, i.e., the speed of sound and adiabatic compressibility of strangeness-neutral strong-interaction matter. These quantities have been calculated previously at vanishing values of the chemical potentials [4,5,16].

We focus on a situation most relevant in the context of heavy ion collision experiments, in which overall net strangeness number density (n_S) vanishes and the ratio of net electric charge (n_Q) to net baryon-number (n_B) densities is close to the isospin-symmetric limit of strangeness neutral matter, $n_Q = n_B/2$. In collisions of heavy nuclei, e.g., gold or lead, the ratio n_Q/n_B is approximately 0.4. Earlier studies of the QCD EoS with a strange quark mass tuned to its physical value, and degenerate light quark masses tuned to reproduce the physical, light hadron spectrum, have been performed for different values of $r \equiv n_Q/n_B$. They have shown that differences in bulk thermodynamic observables, arising from the deviation of r from the isospin-symmetric value, $r = 0.5$, are small [14]. We therefore stick here to an analysis of the thermodynamics of strangeness-neutral, isospin-symmetric systems, which is equivalent to setting the electric charge chemical potential μ_Q to zero.

This paper is organized as follows. In Sec. II we summarize basic thermodynamic relations and outline calculations in QCD with nonvanishing chemical potentials using the Taylor series approach and the resummation of Taylor series using Padé approximants. In Sec. III we present our results on Taylor expansion coefficients for bulk thermodynamic observables and discuss their properties at low and high temperature by comparing with HRG model calculations and $\mathcal{O}(g^2)$ high-temperature perturbation theory, respectively. We furthermore discuss the structure of expansion coefficients in the vicinity of the pseudocritical temperature. In Sec. IV we analyze thermodynamic observables as function of the baryon chemical potential. We determine the baryon chemical potential as function of net baryon-number density to arrive at the QCD equation of state, $P(n_B)$. We furthermore present results for basic thermodynamic observables on the pseudocritical line as well as on lines of constant ratio of entropy to net baryon number. The latter are discussed in Sec. V. We finally give our conclusions in Sec. VI. In three appendices we give some details on directional partial derivatives (A) and discuss $\mathcal{O}(g^2)$ perturbative results for the EoS of strangeness-neutral matter (B) as well as the calculation of the isentropic speed of sound (C).

II. THERMODYNAMICS IN (2+1)-FLAVOR QCD AND GLOBAL CONSTRAINTS

We present here the basic thermodynamic observables that will be analyzed by us in later sections using results from up to eighth-order Taylor expansions of the pressure of QCD with a strange quark mass tuned to its physical value and two degenerate light quark masses that correspond in the continuum limit to a physical pion mass value of about 135 MeV.

We also briefly summarize basic relations used in the Taylor expansion approach to the thermodynamics of QCD at nonzero values of the conserved charge chemical potentials and discuss our approach to the utilization of Padé-resummed Taylor series for thermodynamic observables. Further details on these three topics can be found in [15].

A. Thermodynamic observables

In a grand canonical ensemble the pressure, p, is a function of temperature T and a set of chemical potentials $\vec{\mu} = (\mu_B, \mu_Q, \mu_S)$, which couple to the currents of conserved charges for net baryon number (B), electric charge (Q) and strangeness (S). The pressure is given in terms of the logarithm of the grand canonical partition function

$$\frac{p}{T^4} = \frac{1}{VT^3} \ln \mathcal{Z}(T, V, \hat{\mu}_B, \hat{\mu}_Q, \hat{\mu}_S). \tag{1}$$

We will often use dimensionless variables and observables obtained by rescaling the dimensionful observables with appropriate powers of the temperature, e.g. $\hat{\mu}_X \equiv \mu_X/T$ or $\hat{p} \equiv p/T^4$. With this we obtain for the number densities,

$$\hat{n}_X = \frac{1}{VT^3} \frac{\partial \ln \mathcal{Z}(T, V, \hat{\mu}_B, \hat{\mu}_Q, \hat{\mu}_S)}{\partial \hat{\mu}_X}, \qquad X = B, Q, S, \tag{2}$$

and the energy density,

$$\begin{aligned} \hat{\epsilon} &= \frac{1}{VT^2} \frac{\partial \ln \mathcal{Z}(T, V, \hat{\mu}_B, \hat{\mu}_Q, \hat{\mu}_S)}{\partial T} \\ &= 3\hat{p} + T \frac{\partial \hat{p}}{\partial T}. \end{aligned} \tag{3}$$

The entropy density reads

$$\hat{s} = \hat{\epsilon} + \hat{p} - \hat{\mu}_B \hat{n}_B - \hat{\mu}_Q \hat{n}_Q - \hat{\mu}_S \hat{n}_S. \tag{4}$$

Enforcing the constraint for isospin-symmetric systems, $n_Q = n_B/2$ in strangeness-neutral matter $(n_S = 0)$ is equivalent to demanding $\mu_Q = 0$ [14]. Thermodynamic observables thus become functions of T and $\hat{\mu}_B$ only, i.e., $\hat{p} \equiv p(T, \hat{\mu}_B)/T^4$ and $\hat{s} = \hat{\epsilon} + \hat{p} - \hat{\mu}_B \hat{n}_B$.

In addition to the basic bulk thermodynamic observables introduced above, we also will calculate their temperature derivatives, imposing external constraints. We calculate the isentropic speed of sound in a strangeness-neutral medium with fixed n_Q/n_B, [17],

$$c_s^2 \equiv c_{\vec{X}}^2 = \left(\frac{\partial p}{\partial \epsilon}\right)_{\vec{X}} = \frac{(\partial p/\partial T)_{\vec{X}}}{(\partial \epsilon/\partial T)_{\vec{X}}}. \tag{5}$$

with $\vec{X} = (s/n_B, n_Q/n_B, n_S)$. This also gives the adiabatic compressibility

$$\kappa_s = \frac{1}{n_B}\left(\frac{\partial n_B}{\partial p}\right)_{\vec{X}} = \frac{1}{c_s^2(\epsilon + p - \mu_S n_S)}. \tag{6}$$

The calculation of c_s^2 and κ_s requires taking directional derivatives, which can be done numerically on lines of fixed constraints $\vec{X}$ in the parameter space $(T, \vec{\mu})$, or using analytic relations. Some details on partial derivatives at fixed constraints are given in Appendix A.

B. Taylor expansions

We start with the expansion of the pressure, $\hat{p} = p/T^4$, in terms of the three conserved charge chemical potentials $(\hat{\mu}_B, \hat{\mu}_Q, \hat{\mu}_S)$,

$$\begin{aligned}\hat{p} &= \frac{1}{VT^3} \ln \mathcal{Z}(T, V, \hat{\mu}_B, \hat{\mu}_Q, \hat{\mu}_S) \\ &= \sum_{i,j,k=0}^{\infty} \frac{\chi_{ijk}^{BQS}}{i!j!k!} \hat{\mu}_B^i \hat{\mu}_Q^j \hat{\mu}_S^k,\end{aligned} \tag{7}$$

with $\chi_{000}^{BQS} \equiv p(T,0)/T^4$ and expansion coefficients χ_{ijk}^{BQS},

$$\chi_{ijk}^{BQS} \equiv \chi_{ijk}^{BQS}(T) = \left.\frac{\partial \hat{p}}{\partial \hat{\mu}_B^i \partial \hat{\mu}_Q^j \partial \hat{\mu}_S^k}\right|_{\vec{\mu}=0}. \tag{8}$$

These expansion coefficients are cumulants of conserved charge fluctuations evaluated at vanishing chemical potential.[1]

From this expansion and the constraints, we obtain Taylor expansions for pressure and number densities,

$$\Delta \hat{p} \equiv \frac{p(T, \mu_B)}{T^4} - \frac{p(T,0)}{T^4} = \sum_{k=1}^{\infty} P_{2k}(T) \hat{\mu}_B^{2k}, \tag{9}$$

$$\hat{n}_X = \sum_{k=1}^{\infty} N_{2k-1}^X(T) \hat{\mu}_B^{2k-1}, \qquad X = B, Q, S. \tag{10}$$

The construction of the expansion coefficients,[2] $P_{2k} \equiv \bar{\chi}_0^{B,2k}/(2k)!$ and N_{2k-1} has been discussed previously for the general case of strangeness-neutral matter and a fixed ratio $n_Q/n_B = r$ [14,15]. This gives the chemical potentials $\hat{\mu}_Q$ and $\hat{\mu}_S$ as Taylor series in terms of $\hat{\mu}_B$,

$$\hat{\mu}_Q(T, \mu_B) = q_1(T)\hat{\mu}_B + q_3(T)\hat{\mu}_B^3 + q_5(T)\hat{\mu}_B^5 + \ldots \tag{11}$$

$$\hat{\mu}_S(T, \mu_B) = s_1(T)\hat{\mu}_B + s_3(T)\hat{\mu}_B^3 + s_5(T)\hat{\mu}_B^5 + \ldots. \tag{12}$$

Here we only consider the isospin-symmetric case, $n_Q/n_B = 1/2$, which fixes $\mu_Q = 0$. In that case one finds, for instance, a simple relation between the expansion coefficients of the net baryon-number density and the pressure, $N_{2k-1}^B = 2kP_{2k}$.

Taking derivatives of the expansion coefficients with respect to temperature we also obtain the Taylor series for the energy and entropy densities,

$$\Delta \hat{\epsilon} \equiv \frac{\epsilon(T, \hat{\mu}_B)}{T^4} - \frac{\epsilon(T,0)}{T^4} = \sum_{k=1}^{\infty} \epsilon_{2k}(T) \hat{\mu}_B^{2k}, \tag{13}$$

$$\Delta \hat{s} \equiv \frac{s(T, \hat{\mu}_B)}{T^3} - \frac{s(T,0)}{T^3} = \sum_{k=1}^{\infty} \sigma_{2k}(T) \hat{\mu}_B^{2k}. \tag{14}$$

We note that to obtain Eqs. (13) and (14) one must take the temperature derivatives before applying the constraints. In the case $\mu_Q = 0$, $n_S = 0$, as well as for $\mu_Q = 0$, $\mu_S = 0$ the expansion coefficients are directly related to the expansion coefficients of the Taylor series of the pressure,

$$N_{2k-1}^B(T) = 2kP_{2k}(T), \tag{15}$$

$$\epsilon_{2k}(T) = 3P_{2k}(T) + T\frac{\mathrm{d}P_{2k}(T)}{\mathrm{d}T}, \tag{16}$$

$$\sigma_{2k}(T) = (4 - 2k)P_{2k}(T) + T\frac{\mathrm{d}P_{2k}(T)}{\mathrm{d}T}. \tag{17}$$

We also introduce the notation $\hat{\epsilon}_0 \equiv \epsilon(T,0)/T^4$ and $\hat{\sigma}_0 \equiv s(T,0)/T^3$.

C. Resummation with Padé approximants

In [15] we analyzed the resummation of the Taylor series for the pressure and net baryon-number density using $[n, m]$ Padé approximants. We showed that in the temperature range [135 MeV:175 MeV], the [4, 4] Padé approximants for the pressure have poles only in the complex plane. The location of these poles provide an estimate for the range of validity of the Taylor series. For chemical potentials in this range, one finds good agreement between the Padé approximants and the eighth-order Taylor series for pressure and

---

[1] We often suppress the argument (T) of these generalized susceptibilities and also suppress superscripts and subscripts of χ_{ijk}^{BQS} whenever one of the subscripts vanishes, e.g., $\chi_{i0k}^{BQS} \equiv \chi_{ik}^{BS}$.

[2] See [18] for this notation and explicit definitions of $\bar{\chi}_0^{B,n}$.

net baryon-number density.[3] We will use here the Padé approximants for the Taylor series of the pressure also to determine energy and entropy densities as well as other thermodynamic observables introduced in Sec. II A.

As has been discussed in [15], the Taylor series for the pressure of isospin-symmetric matter with either $\mu_S = 0$ or $n_S = 0$ may conveniently be rewritten as

$$\begin{aligned}\frac{\Delta p(T,\mu_B)}{T^4} &= \frac{P_2^2}{P_4}\sum_{k=1}^{\infty} c_{2k,2}\bar{x}^{2k},\\ &= \frac{P_2^2}{P_4}(\bar{x}^2 + \bar{x}^4 + c_{6,2}\bar{x}^6 + c_{8,2}\bar{x}^8 + \cdots),\end{aligned} \tag{18}$$

with $\bar{x} = \sqrt{P_4/P_2}\hat{\mu}_B$ and

$$c_{6,2} = \frac{P_6 P_2}{P_4^2}, \qquad c_{8,2} = \frac{P_8 P_2^2}{P_4^3}. \tag{19}$$

Using expansion coefficients from fourth, sixth and eighth-order Taylor series for the pressure we construct several $[n,m]$ Padé approximants,

$$P[2,4] = \frac{\bar{x}^2}{1 - \bar{x}^2 + (1 - c_{6,2})\bar{x}^4}, \tag{20}$$

$$P[4,2] = \frac{\bar{x}^2 + (1 - c_{6,2})\bar{x}^4}{1 - c_{6,2}\bar{x}^2}, \tag{21}$$

$$P[4,4] = \frac{(1 - c_{6,2})\bar{x}^2 + (1 - 2c_{6,2} + c_{8,2})\bar{x}^4}{(1 - c_{6,2}) + (c_{8,2} - c_{6,2})\bar{x}^2 + (c_{6,2}^2 - c_{8,2})\bar{x}^4}. \tag{22}$$

The resulting approximants for the pressure are then given by

$$\left(\frac{\Delta p(T,\mu_B)}{T^4}\right)_{[n,m]} = \frac{P_2^2}{P_4} P_{[n,m]}. \tag{23}$$

For the number density we construct the [3, 4] Padé approximant.

Similar Padé approximants can be obtained for the energy density and entropy densities by replacing the expansion coefficients P_{2k} with the corresponding expansion coefficients ϵ_{2k} and σ_{2k}. Rather then constructing in this way Padé approximants for various thermodynamic observables, we also directly determine Padé-based approximants from Eq. (23), using the relevant thermodynamic relations, e.g., Eqs. (3), (4), and (10), for the energy, entropy and net baryon-number densities. The Padé-based approximants, called P-Padé in the following, ensure thermodynamic consistency among different observables and, for instance, ensure that the singularities in the approximations for, n_B/T^3, ϵ/T^4 and s/T^3 coincide with those of the Padé approximation for the pressure. The Padé-based (P-Padé) result for the energy and entropy densities are obtained by taking appropriate partial derivatives of the $[n,m]$ Padé approximation for the pressure with respect to temperature and chemical potential, and using Eqs. (3) and (4),

$$\left(\frac{\Delta\epsilon}{T^4}\right)_{[n,m]} = 3\left(\frac{\Delta p}{T^4}\right)_{[n,m]} + T\frac{\mathrm{d}}{\mathrm{d}T}\left(\frac{P_2^2}{P_4}P_{[n,m]}\right), \tag{24}$$

$$\left(\frac{\Delta s}{T^3}\right)_{[n,m]} = \left(\frac{\Delta\epsilon}{T^4}\right)_{[n,m]} + \left(\frac{\Delta p}{T^4}\right)_{[n,m]} - \hat{\mu}_B\frac{P_2^2}{P_4}\frac{\mathrm{d}P_{[n,m]}}{\mathrm{d}\hat{\mu}_B}. \tag{25}$$

III. TAYLOR EXPANSION COEFFICIENTS OF THE PRESSURE IN (2+1)-FLAVOR QCD

We update here our previous analysis of the EoS of (2 + 1)-flavor QCD performed in lattice QCD calculations with the highly improved staggered quark (HISQ) action and a tree-level improved gauge action [14].

A. Datasets and analysis details

For our calculation of bulk thermodynamic observables we use high-statistics datasets for (2 + 1)-flavor QCD with light and strange quark masses tuned to physical values ($m_\ell/m_s = 1/27$). These datasets have been generated using the HISQ action with tree-level coefficients and a tree-level improved gauge action [14]. Gauge configurations were generated using `SIMULATeQCD` code [20–22]. New datasets exist for the temperature interval [125 MeV:175 MeV] and have been presented in [15]. Additional updates exist for the lowest temperature, where we doubled the number of gauge field configuration to 2.2 M. It is only in this temperature range that 8th order expansion coefficients have been calculated.

Compared to our previous calculation of the EoS [14], the datasets for $N_\tau = 8$ and 12 contain more than an order of magnitude larger statistics and, moreover, include entirely new datasets on lattices with temporal extent $N_\tau = 16$.

At temperatures $T > 180$ MeV, we added to our analysis data from calculations with a slightly larger light quark mass ($m_\ell/m_s = 1/20$), which had been used by HotQCD previously [14]. In all cases results have been obtained on lattices with spatial extent $N_\sigma = 4N_\tau$.

Continuum extrapolations of P_2 and P_4 have been performed in three different temperature intervals, using different ansätze. In the temperature interval [135 MeV: 175 MeV] we use rational polynomial functions as described

---

[3] We note that the recently developed multi-Padé approach [19] provides similar information on the location of poles in the complex plane and may, in the future, also be used to calculate thermodynamic observables.

in [15,23]. The continuum extrapolations for 4th order cumulants follows the same approach as that used for the 2nd order cumulants [15], except it is based on only three different values of the cutoff, i.e., $N_\tau = 6$, 8 and 12. Given our current statistical error for $N_\tau = 12$ data on 4th order cumulants, continuum extrapolations based on $1/N_\tau^2$ as well as $1/N_\tau^2 + 1/N_\tau^4$ corrections agree well within errors. However, since there are no degrees of freedom left when including $1/N_\tau^4$ corrections, we choose to use the $1/N_\tau^2$ extrapolations when quoting errors.

For the high-temperature part $T \geq 175$ MeV, we use a polynomial ansatz to interpolate the data to the continuum limit. Moreover, for low temperatures in the range [125 MeV:145 MeV] we consider an HRG-motivated ansatz, which takes into account the exponential drop of thermodynamic observables at low temperatures and incorporates cutoff-dependent corrections,

$$f(T) = A\left(\frac{B}{T}\right)^{3/2} \mathrm{e}^{-B/T}\left(1 + d_1 T + d_2 T^2 + \frac{c}{N_\tau^2}\right). \qquad (26)$$

Finally, we match all the three functions and their first derivative at $T = 135$ MeV and at $T = 175$ MeV. For the interpolation of P_6 and P_8 we only used spline interpolations of the $N_\tau = 8$ dataset. Much of the data analysis in this study was facilitated through the `AnalysisToolbox` [24]. Statistical uncertainty represented by bands in all figures is calculated through bootstrap resampling. Central values are returned as the median with lower and upper error bounds given by the 32% and 68% quantiles, respectively. Spline interpolations, when needed, are cubic with evenly spaced knots. They are calculated using the `LSQUnivariateSpline` method of SciPy [25]. Central values and error bands shown for the lattice QCD results are smoothed using splines. Temperature derivatives of lattice QCD data are calculated by fitting the temperature dependence with a spline, then calculating the derivative of the spline numerically. We have checked that our spline interpolations and the resulting derivatives are stable under variation of the number of knots used for the interpolation. In general we use splines with 12 knots.

B. Taylor expansion coefficients for the pressure and the trace anomaly

The Taylor series in terms of the conserved charge chemical potentials $\vec{\mu} = (\mu_B, \mu_Q, \mu_S)$ have been reorganized to obtain the Taylor series for the pressure in strangeness-neutral, isospin-symmetric matter given in Eq. (9). Results for the expansion coefficients $(2k)!P_{2k} \equiv \bar{\chi}_0^{B,n}$ are shown in Fig. 1. For the fits and interpolations of different order

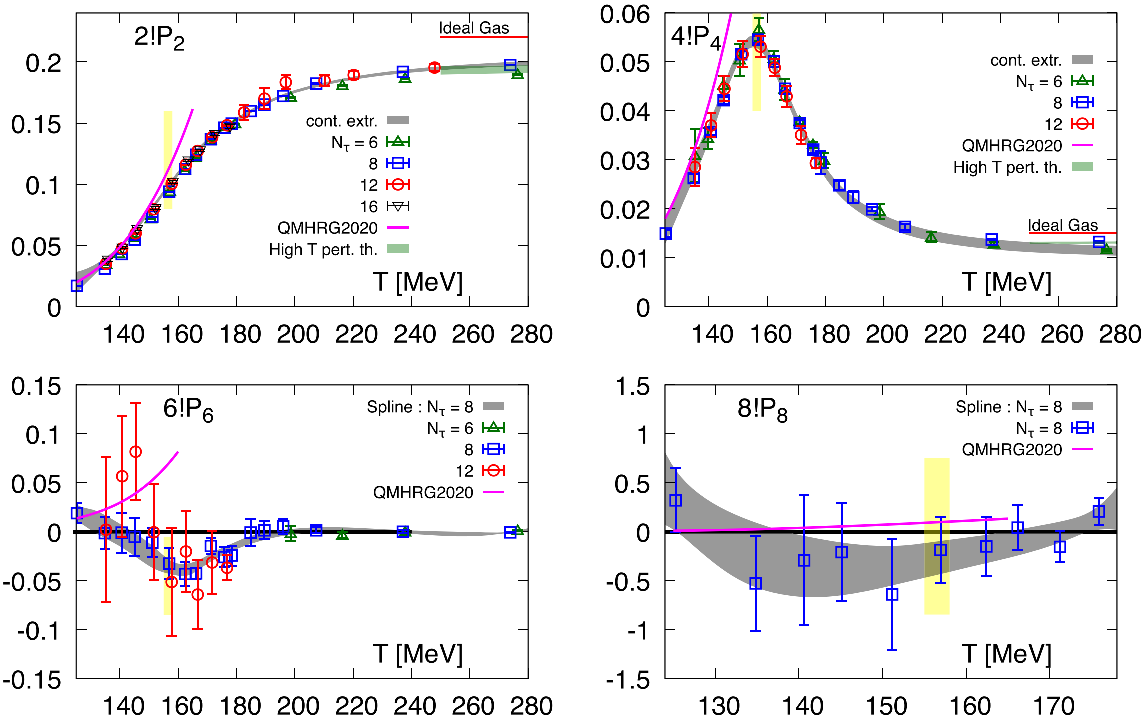

FIG. 1. The nth-order Taylor expansion coefficients, $P_n(T)$, for the Taylor series of the pressure of (2 + 1)-flavor QCD as a function of $\hat{\mu}_B = \mu_B/T$ versus temperature. Shown are the expansion coefficients $n!P_n$ for isospin-symmetric, strangeness-neutral matter ($\mu_Q = 0$, $n_S = 0$). The solid magenta lines show results from a corresponding HRG model calculation using the QMHRG2020 list of hadron resonances [15]. Yellow bands show the location of the pseudocritical temperature $T_{\mathrm{pc}}(0) = 156.5(1.5)$ MeV [28]. The green bands at high temperature show the $\mathcal{O}(g^2)$ perturbative result using a renormalization scale in the range $[4\pi T, 8\pi T]$ (for details see Appendix B).

expansion coefficients shown in this figure we use the same approach as discussed in [15]. I.e., for the $\mathcal{O}(\hat{\mu}_B^2)$ expansion coefficient the band shows a continuum extrapolation based on $N_\tau = 6$, 8, 12, and 16 datasets; for the $\mathcal{O}(\hat{\mu}_B^4)$ expansion coefficient we show a continuum extrapolation based on $N_\tau = 6$, 8 and 12 datasets and for the higher-order expansion coefficients we only use results from our high-statistics calculations on lattices with temporal extent $N_\tau = 8$, where more than 1.5 million gauge field configurations have been generated at each temperature value. In this case the curves show spline interpolations of the $N_\tau = 8$ data. Here we note that the 6th and 8th order expansion coefficients of the pressure have been also estimated using lattice QCD calculations with imaginary chemical potentials in $2+1$ flavor case using $N_\tau = 8$ lattices and stout2 action [26], and in $2+1+1$ flavor case on $N_\tau = 12$ lattices using stout4 action [27]. The qualitative features of the expansion coefficients obtained in these calculations are similar to the ones obtained here.

In the following we discuss several features of the expansion coefficients in the high, low, and intermediate temperatures ranges, respectively.

1. High-temperature region

It is apparent that the expansion coefficients P_{2k} approach the high-temperature ideal gas limit rapidly. In fact, for temperatures $T \gtrsim 250$ MeV, deviations from the ideal gas values are only about 12% for P_2 and P_4. Moreover, at these temperature values the expansion coefficients P_{2k} start being consistent with zero for $k \geq 3$, as is the case in a massless, ideal gas. For $k = 1$ and 2, deviations from the ideal gas limit are well described by $\mathcal{O}(g^2)$ high-temperature perturbation theory, although for a detailed quantitative comparison, refined resummed approaches such as hard thermal loop (HTL) [29] or 3-*d* effective theory (EQCD) [30] may be necessary, as discussed in Refs. [31–33]. In Fig. 1 we show the ideal gas limit result (red line) and $\mathcal{O}(g^2)$ corrections (green band), using a 2-loop running coupling [34] $g^2(T)$ with a renormalization scale $k_T \pi T$ with $4 \leq k_T \leq 8$ as discussed in Appendix B.

For the higher-order expansion coefficients, $k \geq 3$, the ideal gas limit as well as $\mathcal{O}(g^2)$ corrections vanish, which also is consistent with the results shown in Fig. 1.

We also note that for vanishing quark masses, the strange quark sector in strangeness-neutral, isospin-symmetric matter does not contribute to the perturbative expansion of the pressure up to $\mathcal{O}(g^2)$, i.e., although in this case the strangeness chemical potential is nonzero, $\mu_S = \mu_B/3$, the flavor chemical potential for strange quarks vanishes, $\mu_s = 0$. The rapid approach to perturbative behavior of the Taylor expansion coefficients of pressure, and as such also to the $\hat{\mu}_B$-dependent contribution to the pressure, is in contrast to the behavior seen at $\hat{\mu}_B = 0$, where it was found that even at $T \simeq 300$ MeV deviations from the ideal gas limit amount to almost 50% for the pressure and 25% for the energy density [5].

2. Low-temperature region

At low temperatures lattice QCD results for P_2 and P_4 approach results obtained in hadron resonance gas (HRG) model calculations using noninteracting, pointlike resonances. In Fig. 1 QCD results for the pressure coefficients are compared to HRG model calculations that use the QMHRG2020 list of hadron resonances [23]. It is apparent that differences between QCD and HRG model calculations show up earlier and are more pronounced with increasing order of the expansion coefficients. While P_2/P_2^{HRG} deviates from unity by about 10% at $T \simeq T_{\mathrm{pc}}$, this deviation reaches already 50% for P_4/P_4^{HRG}. Moreover, it is evident from the comparison of the temperature dependence of P_4 calculated in QCD and the QMHRG model, respectively, that the slope of $P_4(T)$ differs already significantly for $T > 140$ MeV.

Deviations from HRG model calculations thus are even more apparent in the slope of $P_{2k}(T)$. The T-derivatives, $P'_{2k} = T\mathrm{d}P_{2k}/\mathrm{d}T$, of the expansion coefficients are shown in Fig. 2. As expected $P'_2(T)$ starts deviating from HRG model calculations already at $T \simeq 140$ MeV and differences are about 30% in the vicinity of the pseudocritical temperature, T_{pc}. For $P'_4(T)$ differences are significant in the entire low-temperature region, $T \geq 125$ MeV.

The functions $P'_{2k}(T)$ are the Taylor expansion coefficients of the $\hat{\mu}_B$-dependent part of the trace anomaly,

$$\frac{\Delta(\epsilon - 3p)}{T^4} = \sum_k P'_{2k} \hat{\mu}_B^{2k}. \tag{27}$$

We thus can expect that differences between HRG and QCD results will be larger for energy and entropy densities than for pressure and net baryon-number density as the former two observables receive contributions from $P'_{2k}(T)$. This will be discussed in Sec. III C.

3. Intermediate temperature range: Pseudocritical region

The expansion coefficients shown in Fig. 1, as well as their T-derivatives shown in Fig. 2, make it clear that at temperatures in the vicinity of T_{pc}, deviations from the asymptotic behavior at low and high temperature are large. As has been noted before, the temperature dependence and the relation between subsequent expansion coefficients in the vicinity of T_{pc} resemble many features expected from universal scaling in the vicinity of a second-order phase transition. The maximum in $T\mathrm{d}P_2/\mathrm{d}T$ is close to T_{pc}. In fact, as $P_2(T)$ is an energylike observable [35], its derivative with respect to T,

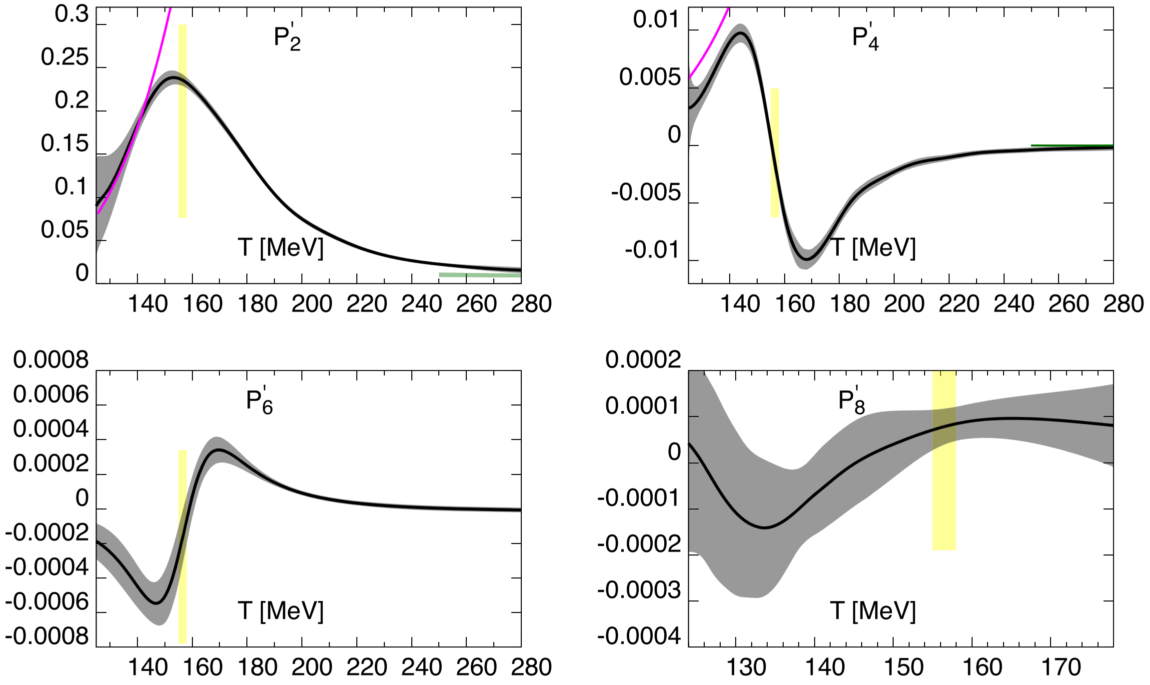

FIG. 2. Derivatives of Taylor expansion coefficients P_2, P_4, P_6, and P_8 with respect to temperature. The solid magenta lines at low temperatures show results from a corresponding HRG model calculation using the QMHRG2020 list of hadron resonances [15]. Yellow bands show the location of the pseudocritical temperature $T_{\rm pc}$ [28] and the green bands at high temperature show the $\mathcal{O}(g^2)$ perturbative result using a renormalization scale in the range $[4\pi T, 8\pi T]$.

$$P_2' = T\frac{\mathrm{d}P_2}{\mathrm{d}T} \equiv \frac{T}{2}\frac{\partial^3 \hat{p}}{\partial T \partial \hat{\mu}_B^2}\bigg|_{\hat{\mu}_B=0}, \qquad (28)$$

behaves like a specific heat, which in the chiral limit will develop a pronounced peak at the chiral phase transition temperature $T_{\rm c}$. This can be used as one of the definitions of a pseudocritical temperature. However, unlike the magnetizationlike susceptibilities, which diverge at $T_{\rm c}$, the energy-like susceptibility will only lead to a local maximum at $T_{\rm c}$. Using the maximum of P_2' as a definition for $T_{\rm pc}$ thus may be more strongly affected by regular contributions to the partition function. Its maximum, on the other hand, characterizes the temperature at which $P_2''(T)$ vanishes. As the maximum and minimum of $P_2''(T)$ on the left and right of this crossing point approach each other and will diverge in the chiral limit, the crossing point itself is a well defined estimator for a pseudocritical temperature. The temperature at this crossing point will converge to the uniquely defined $T_{\rm c}$ in the chiral limit. We find for the location of the maximum of P_2',

$$\mathrm{d}P_2'/\mathrm{d}T = 0 \Rightarrow T_{{\rm pc},P_2} = 153.8(7)(5)\ \mathrm{MeV}, \qquad (29)$$

where the first error is statistical and the second error reflects the uncertainty in defining the T-scale used in all our calculations.

Similarly, the maximum and minimum, visible in P_4' [Fig. 2 (top, right)] will diverge in the chiral limit. The temperature at which P_4' changes sign thus also is a good observable to define a pseudocritical temperature. From the continuum-extrapolated fits shown in Fig. 2 we thus deduce another estimator for $T_{\rm pc}$,

$$P_4' = 0 \Rightarrow T_{{\rm pc},P_4} = 155.3(2)(5)\ \mathrm{MeV}. \qquad (30)$$

Both estimators for $T_{\rm pc}$, based on temperaturelike derivatives of p/T, are in good agreement with results obtained previously by the HotQCD Collaboration using the average over 5 different observables that can be used to define a pseudocritical temperature,[4] i.e., $T_{\rm pc} = 156.5(1.5)$ MeV [28]. Other determinations of pseudocritical temperature, using the zero temperature subtracted chiral susceptibility only [36], gave $T_{\rm pc} = 158.0(6)$ MeV, and a recent, not yet continuum extrapolated, calculation with twisted mass fermions in (2 + 1 + 1)-flavor QCD examined three different definitions of pseudocritical temperature giving results ranging from 146.2(21)(1) MeV to 157.8(7)(10) MeV [37].

The fact that the temperature derivative of P_4, on the one hand, and the temperature derivative of the mixed observable P_2' (involving T- and $\hat{\mu}_B$ derivatives), on the other hand, lead to quite similar results for the value of a pseudocritical temperature is naturally understood in terms of universal behavior in the vicinity of a critical point.

---

[4] Note that pseudocritical temperatures are not unique and depend on the observable used to define them.

Close to T_c higher-order derivatives of the pressure are dominated by the contribution of the so-called singular part of p/T,

$$p/T \sim f_f(z), \tag{31}$$

where f_f is the universal scaling function corresponding to the universality class of the chiral phase transition.[5] The argument z of the scaling function $f_f(z)$ and its prefactor generally depend on the quark masses. However, as we are interested here only in derivatives with respect to T and $\hat{\mu}_B$, keeping the quark masses fixed, we may think of the argument of the scaling function as just being proportional to the reduced temperature t, i.e., $z \equiv c_m t$, with t given by a leading-order Taylor expansion,

$$t = \frac{1}{t_0}\left(\frac{T-T_c}{T_c} + \kappa_2^B \hat{\mu}_B^2 + \mathcal{O}(\hat{\mu}_B^4, \hat{\mu}_B^2(T-T_c), (T-T_c)^2)\right). \tag{32}$$

Here t_0, as well as the chiral phase transition temperature T_c and the curvature coefficient κ_2^B, are nonuniversal parameters. This suggests that up to a proportionality factor, taking two derivatives with respect to $\hat{\mu}_B$ is equivalent to taking one derivative with respect to T [39,40].

The anticipated relation between derivatives with respect to T and $\hat{\mu}_B$, respectively, is apparent in the structure of the expansion coefficients shown in Figs. 1 and 2; P_2' and P_4 receive singular contributions from $f_f''(z)$,

$$\begin{aligned} P_2^{s\prime} &= -\frac{2T}{T_c}\kappa_2^B A f_f''(z) + \text{subleading} \\ P_4^s &= -(\kappa_2^B)^2 A f_f''(z) + \text{subleading}, \end{aligned} \tag{33}$$

where we summarized common factors in the factor $A = (h_0/2t_0^2T^3)h^{-\alpha/\beta\delta}$.

At temperatures in the region between T_c and the pseudocritical temperature for physical quark mass values, the relative magnitude of P_2' and P_4 is well described by scaling relations. Matching values of P_2' and P_4 in the vicinity of T_c thus ensures that their T-derivatives, which will diverge in the chiral limit, will become identical when approaching this limit.

In Fig. 3 we show the expansion coefficient P_4 and compare it with an appropriately rescaled temperature derivative, P_2', of the expansion coefficient P_2. To determine the rescaling factor κ_2^B we calculate the ratio $2TP_4/T_cP_2'$ in the temperature interval [130 MeV:156.5 MeV] and average the results in this interval. As can be seen in the inset of Fig. 3 these estimates increase with increasing T, indicating the relevance of regular contributions to the expansion coefficients P_{2k}, which lead to deviations from a T-independent result for κ_2 that one would expect to find in the scaling regime. For the curvature coefficient we thus find $0.012 \le \kappa_2^B \le 0.022$. This result is in good agreement with other determinations of the curvature coefficient κ_2^B [28,41,42] that are based on properties of magnetizationlike observables.

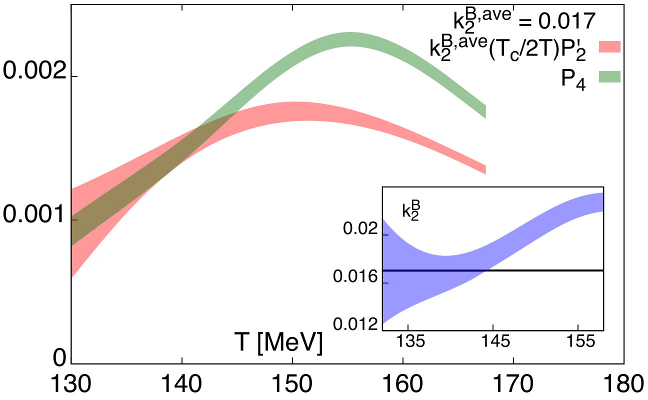

FIG. 3. Comparison of the fourth-order Taylor expansion coefficient, P_4, of the pressure and the temperature derivative of the second-order expansion coefficient, P_2. The red and green bands reflect the errors on P_2' and P_4, respectively. The inset shows results for κ_2^B obtained from an appropriately scaled ratio of P_2' and P_4 as discussed in the text. From this we find $0.012 \le \kappa_2^B \le 0.022$.

C. Taylor expansion coefficients for energy and entropy densities

As discussed in Sec. II B in the case of isospin-symmetric, strangeness-neutral matter, Taylor expansion coefficients of net baryon-number, energy and entropy densities are all given in terms of the expansion coefficients P_{2k} and their temperature derivatives P_{2k}'. In particular, the Taylor series for the $\hat{\mu}_B$-dependent contribution to the trace anomaly $(\epsilon - 3p)/T^4$ is given in terms of the T-derivatives, P_{2k}', only. Combining results for P_{2k} and P_{2k}', shown in Figs. 1 and 2, we then obtain the expansion coefficients for Taylor series of the energy and entropy densities. We show the results for these expansion coefficients, together with those of the pressure series,[6] in Fig. 4. As discussed for the expansion coefficients P_{2k}, also ϵ_{2k} and σ_{2k} are continuum extrapolated for $k = 1, 2$ and we give spline interpolations of the $N_\tau = 8$ results for $k = 3, 4$. We show a comparison with HRG model calculations for the expansion coefficients of the pressure. For energy and entropy we do so only for the second-order expansion coefficients.

---

[5] The chiral phase transition generally is expected to belong to the 3-d, $O(4)$ universality class, although larger symmetry groups may become relevant, if the anomalous $U(1)$ symmetry of QCD gets effectively resorted [38].

[6] Note that the expansion coefficients for the number density are just proportional to those of the pressure series and thus are not shown separately in Fig. 4.

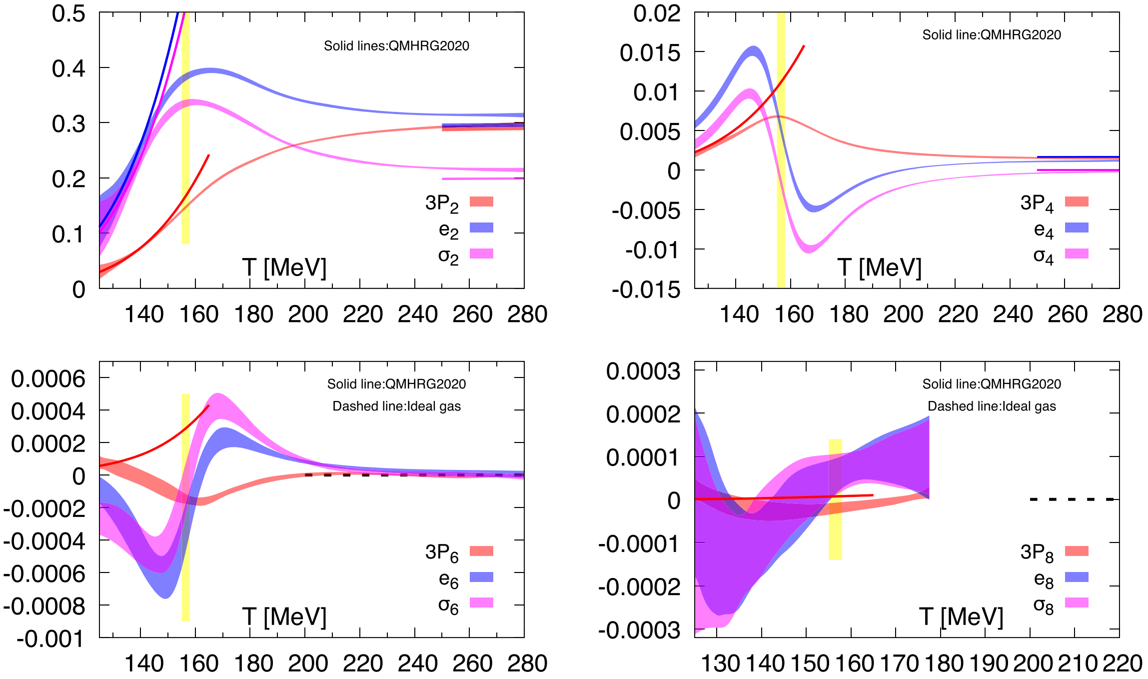

FIG. 4. Second-order (top, left), fourth-order (top, right), sixth-order (bottom, left), and eighth-order (bottom, right) expansion coefficients of pressure (P_{2k}), energy density (ϵ_{2k}), and entropy density (σ_{2k}) for a isospin-symmetric, strangeness-neutral medium ($\mu_Q = 0, n_S = 0$). Bands at high temperature show the $\mathcal{O}(g^2)$ perturbative result using a renormalization scale in the range $[4\pi T, 8\pi T]$. The yellow band indicates the location of the pseudocritical temperature at $T_{\rm pc}$ [28].

As discussed in connection with Fig. 2, differences between HRG model and QCD calculations are large for higher-order expansion coefficients in the entire temperature range.

At high temperatures we again show results from $\mathcal{O}(g^2)$ perturbation theory (PT). In the case of the energy and entropy densities this also includes contributions arising from T-derivatives of the coupling $g^2(T)$, although this might be considered as a part of the $\mathcal{O}(g^4)$ contribution in a perturbative expansion. We thus consider our $\mathcal{O}(g^2)$ PT-ansatz as a model for describing the high-T behavior of the Taylor expansion coefficients and subsequently also for the bulk thermodynamic observables.

IV. BULK THERMODYNAMICS OF (2+1)-FLAVOR QCD

We will use here the Taylor series of the pressure and related observables to calculate thermodynamic observables in an isospin-symmetric, strangeness-neutral medium as function of temperature and baryon chemical potential. Further on, we will eliminate the baryon chemical potential in favor of other external control parameters like the net baryon-number density or constant ratio of entropy over net baryon number.

A. Density dependent contribution to bulk thermodynamic observables

In [15] we already used the new data obtained in the temperature interval $T \in [125\ \text{MeV}: 175\ \text{MeV}]$ to construct 8th-order Taylor series for the pressure and the related 7th-order series for the net baryon-number density. We had shown there that these expansions are reliable for $\hat{\mu}_B \lesssim 2.5$ for the pressure and $\hat{\mu}_B \lesssim 2.0$ for the number density, respectively. It also could be shown that these expansions agree well with corresponding Padé approximants. Here we extend this discussion up to $T = 280$ MeV using existing data from our previous analysis of Taylor series in QCD [14], where a somewhat larger light quark mass, $m_\ell/m_s = 1/20$, has been used in the high-temperature region. Using such a somewhat larger light quark mass at high temperature is of no concern as $m_\ell/T \ll 1$ and has only little influence on thermodynamic observables in this region. We furthermore present results for the energy and entropy densities, which require the temperature derivatives of the expansion coefficients of the pressure.

1. EoS: Pressure versus net baryon-number density

In Fig. 5 we show the number density (right) and the density dependent ($\mu_B \neq 0$) contribution to the pressure (left) for the case $(\mu_Q, n_S) = (0, 0)$ and for several values of $\hat{\mu}_B$. Similar results for the case $(\mu_Q, \mu_S) = (0, 0)$ have been shown in [15]. At high temperatures, $T \gtrsim 200$ MeV, the Taylor series converges rapidly. As can be seen from the expansion coefficients presented in Fig. 1, in this temperature range the 4th-order expansion coefficient, P_4, is more than two orders of magnitude smaller than the 2nd-order

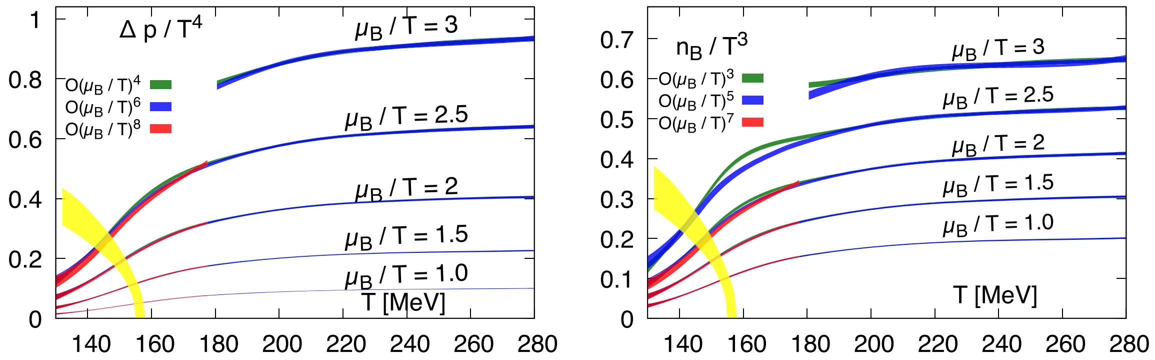

FIG. 5. Pressure (left) and net baryon-number density (right) versus temperature for several values of the baryon chemical potential $\hat{\mu}_B \equiv \mu_B/T$. Shown are results obtained in different orders of the Taylor series of pressure and net baryon-number density of isospin-symmetric, strangeness-neutral matter. The yellow bands highlight the variation of $\Delta p/T^4$ and n_B/T^3 with $\hat{\mu}_B$ at $T_{\mathrm{pc}}(\hat{\mu}_B)$.

coefficient, P_2. Furthermore, within our current statistical accuracy the 6th-order coefficient, P_6, is consistent with zero. Taking into account the statistical error on P_6, also its magnitudes is at least two orders of magnitude smaller than the 4th-order expansion coefficient. For $T \gtrsim 200$ MeV we thus show results for the pressure and net baryon-number density also for larger chemical potentials, e.g., $\hat{\mu}_B \simeq 3$. Using even larger values for $\hat{\mu}_B$ in this high-temperature regime seems to be possible.

For $T \le 200$ MeV contributions from higher-order expansion coefficients become important. The 6th and 8th-order expansion coefficients, which are clearly nonzero, show a lot of structure. Nonetheless, for $T \le 150$ MeV their contribution to the Taylor series of pressure and net baryon-number density is small[7] for $\hat{\mu}_B \le 2.5$. This is in accordance with estimates for the radius of convergence $(\mu_B/T)_{\mathrm{conv}}$ of the Taylor series [15,19,43] that suggest $(\mu_B/T)_{\mathrm{conv}} < 2.5$ also in this temperature range. For further discussion on the radius of convergence of the Taylor series see Refs. [26,44,45]. We also note that in this temperature range and for $\hat{\mu}_B < 2.5$ Taylor series results are consistent within errors with those obtained from the 4th-order series. For temperatures in the vicinity of T_{pc}, i.e., for 150 MeV $< T <$ 200 MeV, contributions from higher-order Taylor expansion coefficients, however, need to be taken into account already for $\hat{\mu}_B > 2$.

This suggests that in the three different temperature intervals 4th and 3rd-order Taylor series provide a good approximation to the 8th-order Taylor series for pressure and net baryon-number density, as long as the baryon chemical potential is smaller than (i) $2.5T$ for $T \le 150$ MeV, (ii) $2T$ for 150 MeV $< T <$ 200 MeV, and (iii) $3T$ for $T \ge 200$ MeV. In these cases we may invert $p(\mu_B)$ and $n_B(T, \mu_B)$ exactly and provide a simple analytic expression for $p(T, n_B)$, which provides useful insight into the structure of the QCD EoS in a parameter range that covers almost the entire parameter range accessible with the beam energy scan (BES-II) at the Relativistic Heavy Ion Collider (RHIC) in collider mode. In particular, at the two lowest beam energies $\sqrt{s_{NN}} = 7.7$ GeV and 11.5 GeV the baryon chemical potentials at the freeze-out temperature $T_f(\mu_B)$ has been estimated to be about $\mu_B/T_f = 2.8$ and 2.0, respectively [46].

Inverting the $\mathcal{O}(\hat{\mu}_B^3)$ Taylor series for the net baryon-number density we obtain the chemical potential as function of T and n_B,

$$\hat{\mu}_B(T, n_B) = y(T, n_B)^{1/3} - \frac{N_1^B(T)}{3N_3^B(T)} y(T, n_B)^{-1/3},$$
$$y(T, n_B) = \frac{N_1^B(T)}{N_3^B(T)} \left(\frac{\hat{n}_B}{2N_1^B(T)} + \sqrt{\frac{N_1^B(T)}{27N_3^B(T)} + \left(\frac{\hat{n}_B}{2N_1^B(T)}\right)^2} \right), \tag{34}$$

where $N_1^B(T) = 2P_2(T)$ and $N_3^B(T) = 4P_4(T)$ are the coefficients of $\mathcal{O}(\hat{\mu}_B^2)$ and $\mathcal{O}(\hat{\mu}_B^4)$ terms in the net baryon-number density, which are obtained either from the Taylor series for net baryon-number density or in $\mathcal{O}(g^2)$ high-temperature perturbation theory.

---

[7] Note that also in a hadron resonance gas, where the $\hat{\mu}_B$-dependent contribution is proportional to $\cosh(\hat{\mu}_B) - 1$, the $\mathcal{O}(\hat{\mu}_B^4)$ Taylor series provides more than 90% of the exact result. Including also the $\mathcal{O}(\hat{\mu}_B^6)$ contribution results in agreement with the exact HRG result to better than 1% for $\hat{\mu}_B \le 2.5$.

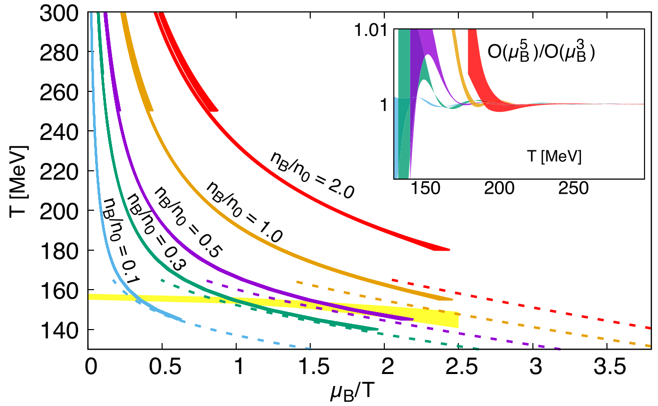

FIG. 6. Lines of constant net baryon-number density in the $\hat{\mu}_B$-T plane. Solid bands indicate results obtained by numerically solving the $\mathcal{O}(\hat{\mu}_B^5)$ series of $\hat{n}_B$ for $\hat{\mu}_B$. Dashed lines indicate HRG results while short bands at high temperature indicate the $\mathcal{O}(g^2)$ perturbative result with $4 \le k_T \le 8$. The yellow band indicates $T_{\rm pc}(\hat{\mu}_B)$. In the inset, we show the result from numerically inverting the Taylor series divided by the analytic inversion of the $\mathcal{O}(\hat{\mu}_B^3)$ result.

Inserting these results for the chemical potential in the 4th-order Taylor series for the pressure we obtain a low-order approximation for the EoS of strangeness-neutral matter, i.e., $p(T, n_B)$,

$$\frac{\Delta p(T, n_B)}{T^4} = P_2(T)\hat{\mu}_B^2(T, n_B) + P_4(T)\hat{\mu}_B^4(T, n_B). \tag{35}$$

Going beyond the low-order approximation for the EoS we can solve $\hat{n}_B(T, \hat{\mu}_B)$ numerically for $\hat{\mu}_B$ at fixed T. We then obtain $\hat{\mu}_B(T, n_B)$, which can be inserted in the 8th-order Taylor series for $p(T, \hat{\mu}_B)$ and thus allows us to determine $p(T, n_B)$.

In Fig. 6 we show results for lines of constant net baryon-number density in the $\hat{\mu}_B$-T plane. Results are shown for several values of n_B/n_0, with $n_0 = 0.16/\mathrm{fm}^3$ denoting nuclear matter density. They are compared to QMHRG model calculations at low T and $\mathcal{O}(g^2)$ perturbation theory at high T, respectively. The inset shows a comparison of the numerically inverted Taylor series result and the exact inversion of the 3rd-order Taylor series for $\hat{n}_B(\hat{\mu}_B)$ given in Eq. (34). Here we show results only in T-intervals where $\hat{\mu}_B$ stays below the maximal values given above. As can be seen, the temperature dependence of $\hat{\mu}_B$ characterizing lines of constant n_B are well determined from the $\mathcal{O}(\hat{\mu}_B^3)$ Taylor series for the net baryon number-density for $\hat{\mu}_B \le 2.5$.

Inserting $\hat{\mu}_B(T, n_B)$ in the Taylor series for the pressure we obtain the contribution to the QCD EoS of strangeness-neutral, isospin-symmetric matter that depends on nonzero net baryon number density. Results for $\Delta p/(n_B T)$ as function of n_B/T^3 for several values of T are shown in Fig. 7 (left). Again we only show results for $\Delta p/(n_B T)$ for values of n_B/T^3 which correspond to $\hat{\mu}_B \le 2.5$ for $T \le 200$ MeV and $\hat{\mu}_B \le 3$ for $T > 200$ MeV. In Fig. 7 (left) we show corresponding results as function of n_B/n_0.

For $T \gtrsim 240$ MeV it is evident that $\Delta p(T, n_B)/(T n_B)$, rises almost linearly in n_B/T^3 and is close to the ideal gas result. I.e., $\Delta p(T, n_B)$ is proportional to $(n_B/T)^2$. In this temperature range the density-dependent part of the QCD EoS is not only close to the ideal gas result, but also agrees rather well with the $\mathcal{O}(g^2)$ perturbative EoS already for $T \ge 220$ MeV. This is shown by the gray bands in Fig. 7 (right) for which we used the $\mathcal{O}(g^2)$ perturbative EoS for the case $(\mu_Q, n_S) = (0, 0)$, given in Appendix B, with a renormalization scale $k_T \pi T$, using $4 \le k_T \le 8$.

From Eqs. (34) and (35) we expect at low densities to find $\Delta p \sim (n_B/T)^2$. The notion of low density, however, is temperature dependent. As can be seen from Eq. (34), the leading order coefficient $N_1^B(T)$ sets the scale for n_B. As $N_1^B(T)$ drops exponentially at low temperature one quickly enters a region of "high density" already at densities

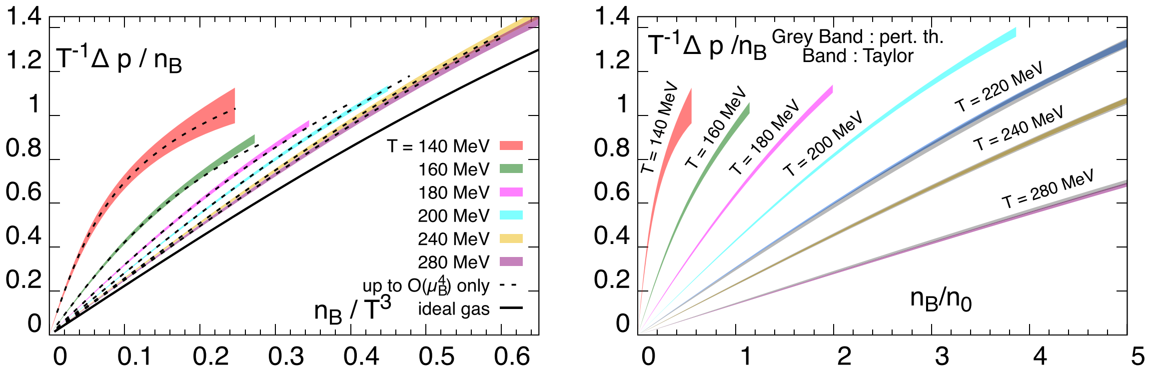

FIG. 7. Pressure divided by net baryon-number density versus n_B/T^3 (left) and n_B/n_0 (right), respectively. Shown are results for strangeness-neutral, isospin-symmetric matter at several values of T. In the left hand figure we compare results obtained from the full Taylor series for the pressure with those obtained in $\mathcal{O}(\hat{\mu}_B^4)$ only (dashed lines). In the right hand side the gray bands show a comparison with $\mathcal{O}(g^2)$ high-T perturbation theory. The bands shown in both figure are shown up to values of n_B/T^3 or n_B/n_0 corresponding to $\hat{\mu}_B = 2.5$ for $T < 200$ MeV and $\hat{\mu}_B = 3$ otherwise.

smaller than nuclear matter density, $n_0 \simeq 0.16\ \mathrm{fm}^{-3}$, whereas at high temperature the low density regime ($\Delta p \sim (n_B/T)^2$) persists into a region well above n_0.

At low densities we thus expect that the density dependent contribution (Δp) to the total pressure is proportional to $(n_B/T)^2$ while the n_B-dependence weakens. At high densities and, within the approximation given by Eq. (35), one finds $\Delta p \sim n_B^{4/3}$.

Results for $\Delta p(T, n_B)/n_B$, obtained with this $\mathcal{O}(\hat\mu_B^4)$ approximation (dashed lines), are compared with the full Taylor series results (bands) in Fig. 7 (left). The bands are shown up to a maximal density that can be reliably reached with our current 8th-order Taylor series in different temperature regions, i.e., we demand that $\hat\mu_B \le 2.5$ for $T \le 200$ MeV and $\hat\mu_B \le 3$ at higher temperatures. As can be seen the dashed lines indeed provide a good approximation for the EoS at temperatures $135\ \mathrm{MeV} < T \le 150$ MeV and for $T \ge 200$ MeV. Only for $150\ \mathrm{MeV} < T < 200$ MeV we find that an EoS based on the 4th-order Taylor series is not sufficient. Here differences become visible in a region corresponding to $\hat\mu_B > 2$.

2. *Energy and entropy densities*

The calculation of Taylor series for the energy and entropy densities requires the derivatives of Taylor expansion coefficients of the pressure with respect to temperature, $P'_{2k} \equiv T\mathrm{d}P_{2k}/\mathrm{d}T$. These expansion coefficients are shown in Fig. 2. They directly give the Taylor series for the $\hat\mu_B$-dependent contribution to the trace anomaly, as introduced in Eq. (27). In Fig. 8 we show $\Delta(\epsilon - 3p)/T^4$ for several values of the baryon chemical potential. This should be compared to the trace anomaly at $\hat\mu_B = 0$ (Fig. 5 (right) of [5]). We note that at T_{pc} and for $\hat\mu_B = 2.5$ the fermionic contribution to the trace anomaly is as large as the contribution at $\hat\mu_B = 0$ but rapidly drops at larger values of the temperature. For $T \ge 200$ MeV the $\hat\mu_B$-dependent contribution to the trace anomaly stays below 10% of the value of the trace anomaly at $\hat\mu_B = 0$.

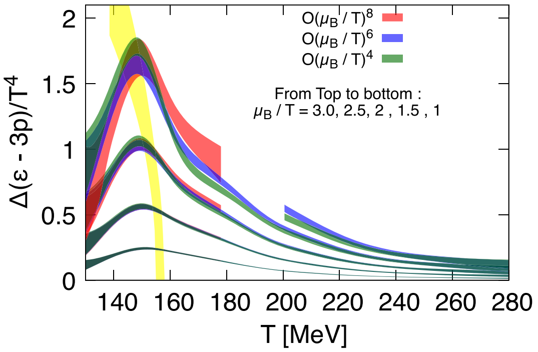

FIG. 8. The $\hat\mu_B$-dependent contribution to the trace anomaly in (2 + 1)-flavor QCD for several values of $\hat\mu_B$. The yellow band shows the line $\Delta((\epsilon - 3p)/T^4)(T_{\mathrm{pc}}(\hat\mu_B))$.

A consequence of this is that the maximum in the trace anomaly, which at $\hat\mu_B = 0$ is reached at $T \simeq 200$ MeV [5], gets shifted to smaller temperatures and comes closer to the pseudocritical temperature. In fact, as can be seen in Fig. 8, the location of the maximum of $\Delta(\epsilon - 3p)/T^4$ is close to the pseudocritical temperature determined from chiral observables,

$$T_{\mathrm{pc}}(\hat\mu_B) = T_{\mathrm{pc}}^0 (1 - \kappa_2^{B,f} \hat\mu_B^2 + \mathcal{O}(\hat\mu_B^4)), \qquad (36)$$

with $T_{\mathrm{pc}}^0 = 156.5(1.5)$ MeV and $\kappa_2^{B,f} = 0.012(4)$ denoting the curvature coefficient of the pseudocritical line in strangeness-neutral matter[8] [28]. For large values of the chemical potential, where $\Delta(\epsilon - 3p)/T^4$ is dominated by the $\hat\mu_B$-dependent contribution, violations of the conformal relation $\epsilon = 3p$ thus are maximal on the pseudocritical line.

Combining the results for $\Delta(\epsilon - 3p)/T^4$ (Fig. 8) and $\Delta p/T^4$ (Fig. 5) we obtain the Taylor series results for the $\hat\mu_B$-dependent contributions to ϵ/T^4 and s/T^3, respectively. These observables are shown in Fig. 9. As discussed in the case of $\Delta p/T^4$ and n_B/T^3, we also find for $\Delta(\epsilon - 3p)/T^4$, as well as for $\Delta\epsilon/T^4$ and $\Delta s/T^3$, that the 4th-order Taylor expansions provide good approximations to the full 6th and 8th-order series results for $T \ge 200$ MeV and $T \le 150$ MeV whenever $\hat\mu_B \le 2.5$ in the low-T region and $\hat\mu_B \le 3$ at high T. Higher-order corrections become more important in the calculation of the entropy density at high temperature. As can be seen in Fig. 9 (right) the 6th and 4th-order correction to s/T^3 agree with each other in the region $T > 200$ MeV only up to $\hat\mu_B \simeq 2.5$ but start to differ for larger $\hat\mu_B$.

As can be seen in Fig. 9 for large $\hat\mu_B$ the 4th-order Taylor expansion results for $\Delta\epsilon/T^4$ and $\Delta s/T^3$ show a wiggly behavior in the intermediate temperature interval, $150\ \mathrm{MeV} < T < 200$ MeV, which results from the pronounced minimum of P'_4 in this temperature interval. This structure gets smoothed out by higher-order corrections. We will show in the next subsection that a Padé-resummed Taylor series shows a much smoother behavior in this temperature range.

We use the 6th-order Taylor expansion results for $\Delta p/T^4$, $\Delta\epsilon/T^4$, and $\Delta s/T^3$ to obtain the latter two as functions of T and n_B. We again compare with corresponding 4th-order approximations using,

$$\frac{\Delta\epsilon(T, \hat n_B)}{T^4} = \epsilon_2(T)\hat\mu_B^2(T, n_B) + \epsilon_4(T)\hat\mu_B^4(T, n_B), \qquad (37)$$

$$\frac{\Delta s(T, \hat n_B)}{T^3} = \sigma_2(T)\hat\mu_B^2(T, n_B) + \sigma_4(T)\hat\mu_B^4(T, n_B), \qquad (38)$$

---

[8] For a summary of different determinations of the curvature coefficient κ_2^B, using various external constraints, see for instance [36,47].

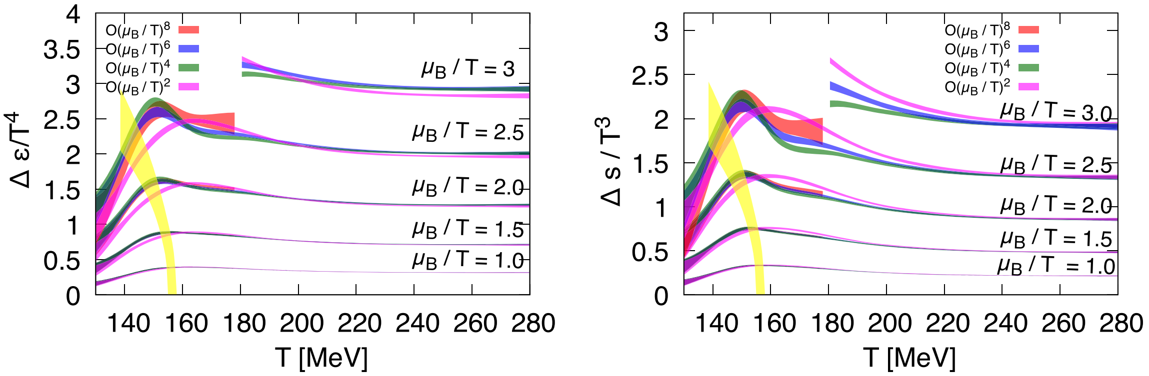

FIG. 9. $\hat{\mu}_B$-dependent part of the energy (left) and entropy (right) densities versus temperature. Shown are results from 2nd, 4th, 6th, and 8th-order Taylor expansions. The yellow bands indicate how $\Delta\epsilon/T^4$ and $\Delta s/T^3$ change with $\hat{\mu}_B$ at $T_{\rm pc}$.

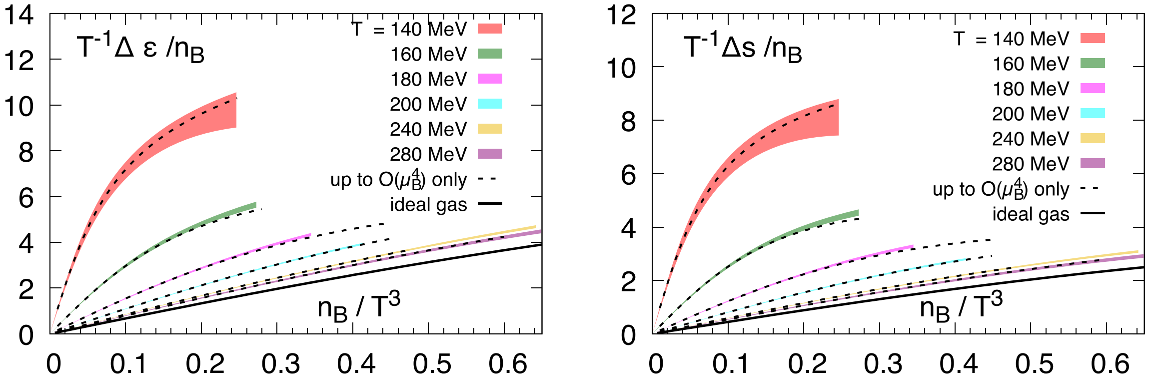

FIG. 10. Energy density in units of T^4 divided by net baryon-number density versus n_B/T^3 (left) and the corresponding figure for entropy density (right). Shown are results for strangeness-neutral, isospin-symmetric matter at several values of T using 6th-order Taylor expansions for ϵ/T^4 and s/T^3 and a 5th-order Taylor expansions for n_B/T^3. Dashed lines show a comparison with results based on 4th and 3rd-order expansions, respectively, using Eq. (34) to obtain $\epsilon(n_B)$ and $s(n_B)$.

with $\hat{\mu}_B(T,\hat{n}_B)$ taken from Eq. (34). Results for $\Delta\epsilon(T,\hat{n}_B)/n_B$ and $\Delta s(T,\hat{n}_B)/n_B$ as functions of $\hat{n}_B$ are shown in Fig. 10.

3. Comparison of Taylor series and their resummation using Padé approximants

As seen already in the analysis of the Taylor expansion for the pressure and net baryon-number density, Padé approximants agree well with the Taylor series themselves at low $\hat{\mu}_B$ up to the region where we estimated the latter to provide reliable results [15]. We will extend this approach here to the analysis of Taylor series for the energy and entropy densities.

We use Padé approximants for thermodynamic observables derived from the Taylor series of the pressure in two ways. On the one hand we construct Padé approximants based on the Taylor series for a given observable, e.g., the energy and entropy density series given in Eqs. (13) and (14) can be resummed using Padé approximants similar to that of the pressure series given in Eq. (23) by just replacing the expansion coefficients P_{2k} by ϵ_{2k} or σ_{2k}, respectively. On the other hand we use the P-Padé, i.e., appropriate derivatives of the Padé approximants for the pressure, for the energy and entropy densities as given in Eqs. (24) and (25).

In Fig. 11 (left) we compare 6th and 8th-order Taylor series for $\Delta\hat{p}$ with corresponding [4, 2], [2, 4], and [4, 4] Padé approximants introduced in Eqs. (20)–(23). Corresponding results for $\Delta\hat{\epsilon}$ are shown in Fig. 11 (right). In the figure for the pressure (top, left) we compare the 6th-order Taylor expansion results with the two possible $[n,m]$ Padé approximants that use up to 6th-order expansion coefficients. As can be seen the [4, 2] Padé agrees with the Taylor series result while the [2, 4] Padé differs from these two in the temperature interval 150 MeV $\lesssim T \lesssim$ 180 MeV. In the (bottom, left) figure shows a comparison of the 8th-order Taylor expansion results with the [4, 4] Padé approximant. They are in good agreement with each other. Moreover, as can be seen from the inset, for large values of $\hat{\mu}_B$ the [2, 4] and [4, 4] Padé approximants stay in much better agreement with each other than the [4, 2] and [4, 4] Padé approximants or, equivalently, the 6th and 8th-order Taylor series. Similar conclusions can be drawn for the energy density shown in the right hand part of the figure.

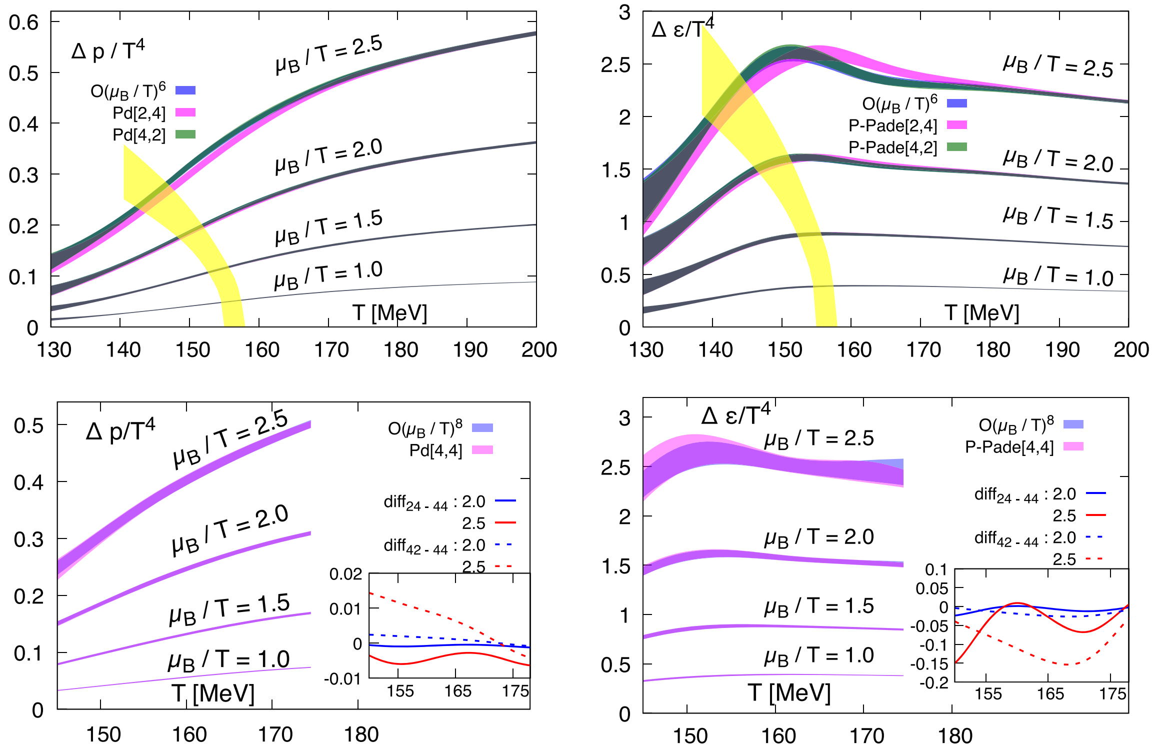

FIG. 11. Comparison of 6th (top) and 8th (bottom) order Taylor expansion results for $\Delta p/T^4$ and $\Delta\epsilon/T^4$ with corresponding [2, 4] and [4, 4] Padé and P-Padé approximants. The inset in the bottom panels shows differences in the [2, 4] and [4, 4] as well as in [4, 2] and [4, 4] Padé approximations, which are all based on 8th-order Taylor series. The yellow bands highlight the variation of $\Delta p/T^4$ and $\Delta\epsilon/T^4$ with $\hat{\mu}_B$ at $T_{\rm pc}(\hat{\mu}_B)$.

In Fig. 12 we compare at fixed values of the temperature 8th-order Taylor expansion results with the [4, 4] Padé approximant as well as the P-Padé results for pressure, energy and entropy densities that we have discussed above and in Sec. II C. We generally find that the P-Padé results for bulk thermodynamic observables are in better agreement with the Taylor series results than the [4, 4] or [3, 4] Padé approximants. This may not be too surprising, as both approaches are based on a thermodynamically self-consistent set of expressions.

We consider results for bulk thermodynamic observables based on the 8th-order Taylor series for the pressure reliable when the Taylor series results agree with the [4, 4] Padé approximants as well as the P-Padé approximants shown in Fig. 12. These parameter ranges are similar for all four bulk thermodynamic observables shown in Fig. 12 and also agree with current estimates for a radius of convergence of the Taylor series given in [15,19,43]. We thus conclude that the region of reliability of current EoS results is slightly temperature dependent, increasing from $\hat{\mu}_B \simeq 2.2$ at $T = 135$ MeV to $\hat{\mu}_B \simeq 3.2$ at $T = 180$ MeV. The latter also holds for higher values of the temperature where our results only are based on 6th-order Taylor series expansions.

B. Bulk thermodynamic observables

Having discussed the μ_B-dependent contribution to bulk thermodynamic observables in the previous subsection we can now combine these results with those obtained at vanishing values of the chemical potential, for which we use the continuum-extrapolated results obtained for (2 + 1)-flavor QCD by the HotQCD collaboration [5].

In Fig. 13 we show the total pressure (left) as well as energy (middle) and entropy (right) densities for $\hat{\mu}_B \in [0:2.5]$ in the entire temperature range analyzed by us. For $\hat{\mu}_B = 3$ we show results in the region $T \geq 180$ MeV only.

Also shown in Fig. 13 are results from HRG model calculations for $\hat{\mu}_B = 0$ and 2.5. It is apparent that the HRG model results show a stronger $\hat{\mu}_B$-dependence than the QCD data. Already in the vicinity of $T_{\rm pc}$ differences between HRG model calculations and QCD increase with increasing values of $\hat{\mu}_B$. This is to be expected as higher-order Taylor expansion coefficients start to differ from HRG model results already at rather low temperatures, $T < 140$ MeV, and differences get large in the transition region (see Fig. 4). These differences are larger for the energy and entropy densities than for pressure and number density. In particular, we find that the $\mathcal{O}(\hat{\mu}_B^2)$ coefficients in QCD are about 30% smaller than in HRG model calculations (see Fig. 4) and the ratio of $\mathcal{O}(\hat{\mu}_B^4)$ and $\mathcal{O}(\hat{\mu}_B^2)$ expansion coefficients of the energy density calculated in lattice QCD and HRG models, respectively, differs by almost a factor 5, i.e., $\epsilon_4(T_{\rm pc})/\epsilon_2(T_{\rm pc}) = 0.013(2)(6)$ in QCD compared to $(\epsilon_4(T_{\rm pc})/\epsilon_2(T_{\rm pc}))_{\rm HRG} = 0.065(1)$ in the

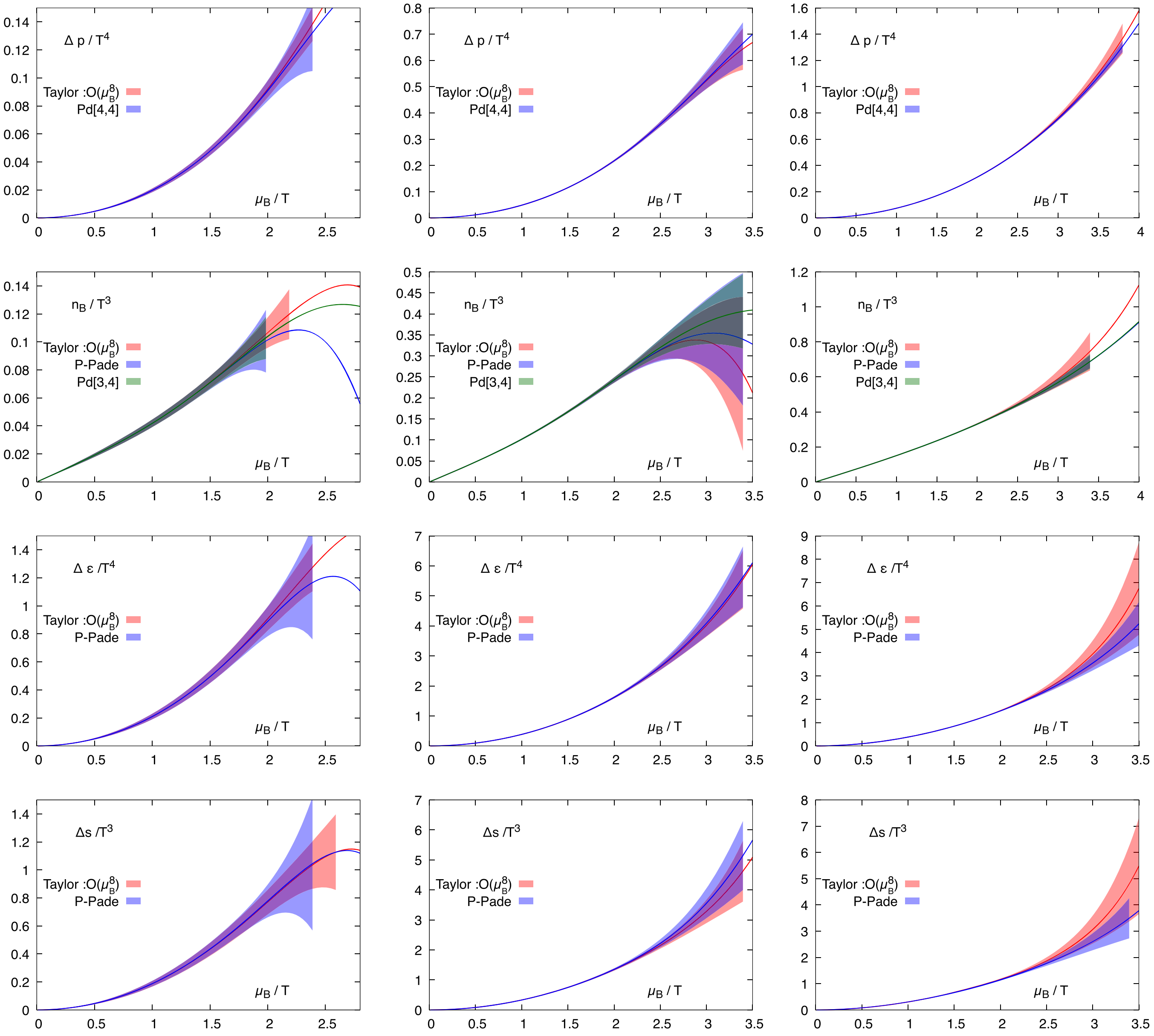

FIG. 12. Top to bottom: comparison of Taylor series and Padé approximants for pressure, net baryon-number, energy, and entropy densities, at three values of the temperature, $T = 135$ MeV (left), 155 MeV (middle), and 175 MeV (right). Taylor expansion results are shown for 8th and 7th-order (number density), respectively. The corresponding Padé approximants are [4, 4] and [3, 4]. Also shown are P-Padé approximants (P-Pade) which are appropriate T- and μ_B-derivatives of the [4, 4] Padé approximant for the pressure as discussed in Sec. II C.

HRG model, using the QMHRG2020 hadron list. As a consequence, with increasing $\hat{\mu}_B$ the difference between the energy density calculated in QCD and HRG models increases on the pseudocritical line, $T_{\rm pc}(\hat{\mu}_B)$.

As discussed in [14], the curvature coefficients κ_2^ϵ and κ_2^s for lines of constant energy and entropy densities, respectively, are related through the second-order expansion coefficients σ_2 and s_2,

$$\frac{\kappa_2^s}{\kappa_2^\epsilon} = \frac{\sigma_2}{\epsilon_2} = 1 - \frac{P_2}{\epsilon_2} = 0.872(3)(5). \qquad (39)$$

Lines of constant energy density thus are flatter than those for constant entropy density, i.e., the entropy decreases on a line of constant energy density. Using the coefficients ϵ_2 and σ_2, shown in Fig. 4, we get

$$\kappa_2^\epsilon = 0.0104(12), \qquad \kappa_2^s = 0.0091(11), \qquad (40)$$

which should be compared to the curvature coefficient $\kappa_2^{B,f}$ of the pseudocritical line given in Eq. (36). These results thus suggest that, within current statistical errors, energy

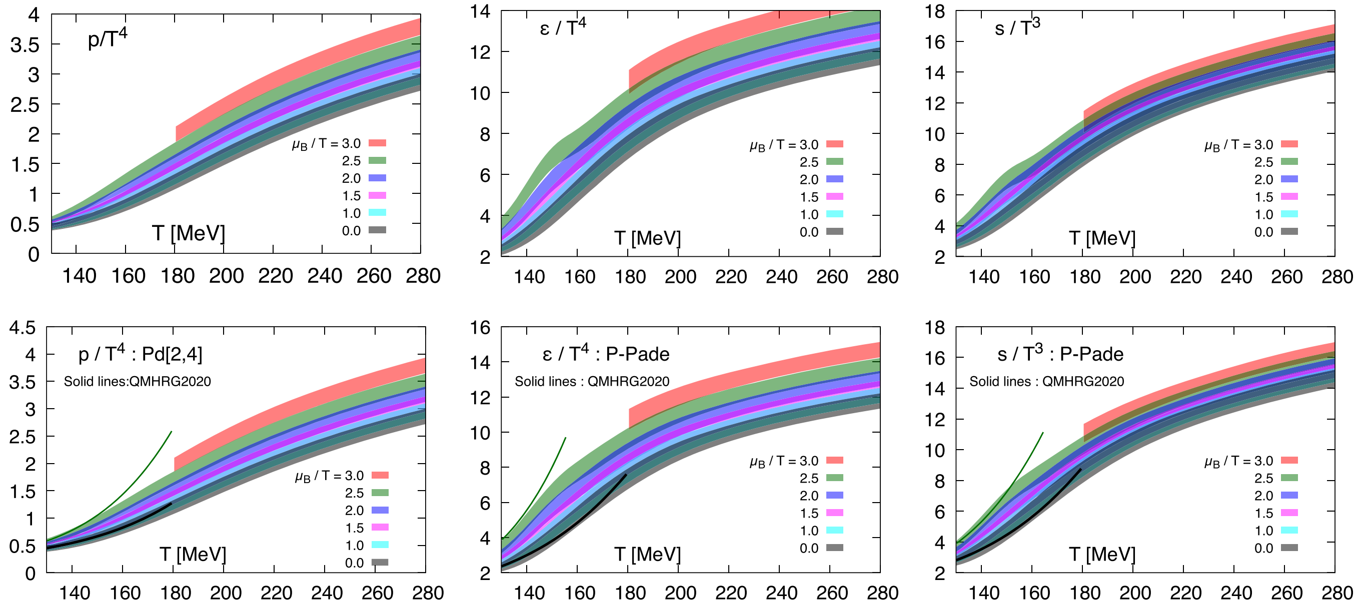

FIG. 13. Pressure (left) as well as energy (middle) and entropy (right) densities versus temperature for several values of the baryon chemical potential. Figures show results for the case $n_S = 0$, $n_Q/n_B = 0.5$ in the temperature interval [130 MeV:280 MeV]. Figures on the top show results from 6th order Taylor series and the figures on the bottom have been used using Padé and P-Padé approximants, respectively. The Taylor expansions are based on the continuum and spline interpolated data shown in Fig. 1 for the temperature interval [130 MeV:175 MeV]. At larger temperatures we used data from our earlier analysis of bulk thermodynamics in a sixth-order Taylor expansion [14]. Results for $\hat{\mu}_B = 0$ have been taken from [5].

and entropy densities stay constant on the pseudocritical line or drop slightly.

Using the results for ϵ/T^4 shown in Fig. 13 (middle) we find for the energy density on the pseudocritical line,

$$\epsilon(T_{\mathrm{pc}}(\hat{\mu}_B)) = \begin{cases} 370(40)(30)\ \mathrm{MeV/fm^3}, & \hat{\mu}_B = 0 \\ 330(28)(53)\ \mathrm{MeV/fm^3}, & \hat{\mu}_B = 2.5 \end{cases}. \tag{41}$$

Here the first error is the statistical error on ϵ at $T_{\mathrm{pc}}(\hat{\mu}_B)$, while the second error reflects the systematic uncertainty arising from the uncertainty on $T_{\mathrm{pc}}(\hat{\mu}_B)$, which rises from 1.5 MeV at $\hat{\mu}_B = 0$ to 4 MeV at $\hat{\mu}_B = 2.5$.

V. THERMODYNAMICS AT CONSTANT RATIO OF ENTROPY TO NET BARYON NUMBER

Equilibrated strong interaction matter created, for instance in heavy ion experiments, follows lines of constant entropy per net baryon number while expanding and cooling after the initial collision of nuclei. The composition of the initially colliding nuclei thus fixes the conserved charge content of the matter created in this collisions, i.e., $n_S = 0$ and n_Q/n_B fixed.

Also for the calculation of thermodynamic observables such as the speed of sound or the adiabatic compressibility of matter, one needs to determine the lines of constant s/n_B in QCD [11,13]. We have determined the lines of constant s/n_B in a strangeness-neutral medium with fixed n_Q/n_B.

In Fig. 14 we show such lines in the $\hat{\mu}_B$-T plane for s/n_B and fixed $(n_S, n_Q/n_B) = (0, 0.5)$ in the range $25 \le s/n_B \le 400$. This roughly corresponds to the range covered by BES-II at RHIC in the range of beam energies 7.7 GeV $\le \sqrt{s_{NN}} \le$ 200 GeV. Also shown in Fig. 14 is the asymptotic behavior of lines of constant n_B at high

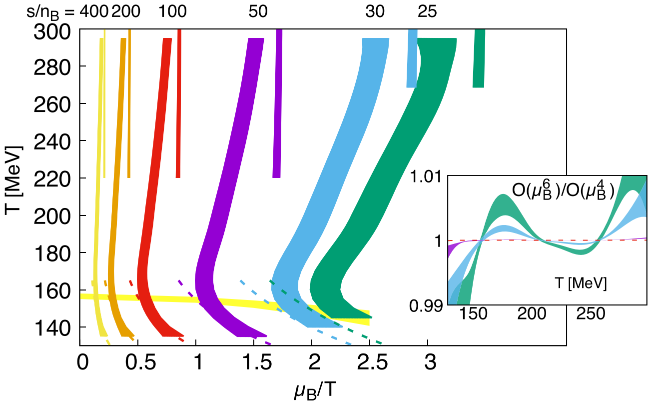

FIG. 14. Lines of constant entropy per baryon number in the T-$\hat{\mu}_B$ plane. Solid bands indicate results obtained by numerically solving s/n_B derived from the $\mathcal{O}(\hat{\mu}_B^6)$ pressure series for $\hat{\mu}_B$. Dashed lines indicate HRG results while the (almost straight) vertical bands indicate the $\mathcal{O}(g^2)$ perturbative result with $4 \le k_T \le 8$. The yellow band indicates $T_{\mathrm{pc}}(\hat{\mu}_B)$. In the inset, we show the result from this numerical inversion divided by the corresponding inversion coming from the $\mathcal{O}(\hat{\mu}_B^4)$ pressure series.

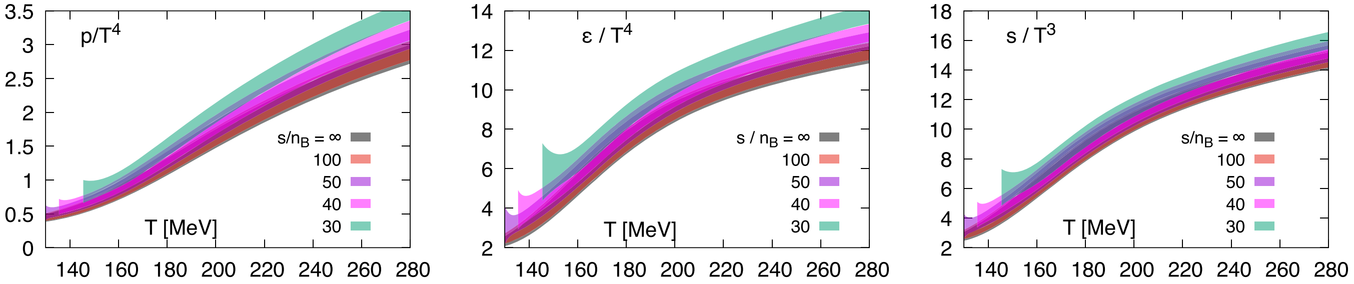

FIG. 15. Total pressure (left), energy density (middle), and entropy density (right) versus temperature for several values of the ratio s/n_B.

temperature and the approach to the HRG model at low temperature. As can be seen, QCD results for lines of constant s/n_B differ much more from high-T perturbation theory then the lines of constant n_B. This, of course, arises from the $\mu_B = 0$ contribution to the total entropy density, which approaches the ideal gas limit slowly. The inset in Fig. 14 shows that these lines are already well determined using 4th order Taylor series only.

In Fig. 15 we show the temperature dependence of pressure, energy and entropy densities on lines of constant s/n_B. Obviously, the T-dependence of these observables is similar to that obtained for fixed $\hat{\mu}_B$. Above the pseudocritical temperature, however, these observables rise somewhat faster than at $\mu_B = 0$, i.e., at $s/n_B = \infty$. This is expected as Fig. 14 shows that the value of the chemical potential on lines of constant s/n_B increases above $T_{\rm pc}$ with increasing temperature.

The speed of sound in strangeness-neutral matter with fixed n_Q/n_B reflects the temperature dependence of p and ϵ, shown in Fig. 15. As defined in Eq. (5) we have,

$$c_s^2 = \left(\frac{\partial p}{\partial \epsilon}\right)_{s/n_B, n_Q/n_B, n_S} = \frac{(\partial p/\partial T)_{s/n_B, n_Q/n_B, n_S}}{(\partial \epsilon/\partial T)_{s/n_B, n_Q/n_B, n_S}}. \tag{42}$$

The numerator is related to the entropy density evaluated at fixed $\vec{X} = (s/n_B, n_Q/n_B, n_S)$, while the denominator is a specific heat defined at fixed $\vec{X}$. We note, however, that the temperature derivatives taken at fixed $\vec{X}$ differ, of course, from those taken at fixed $\vec{\mu}$. Some relations for constrained partial derivatives are given in Appendices A and C we give an explicit expression for c_s^2.

For $n_S = 0$ we obtain from Eqs. (5) and (6) for the speed of sound (c_s^2) and the closely related adiabatic compressibility (κ_s)

$$c_s^2 = \frac{N_{\vec{X}}}{(\epsilon + p) D_{\vec{X}}}, \qquad \kappa_s = \frac{1}{c_s^2(\epsilon + p)} = \frac{D_{\vec{X}}}{N_{\vec{X}}}. \tag{43}$$

The functions $N_{\vec{X}}(T, \vec{\mu})$ and $D_{\vec{X}}(T, \vec{\mu})$ are given in terms of second-order cumulants of the conserved charges (B, Q, S), the entropy density and its derivatives with respect to T as well as the three chemical potentials. All these observables themselves are functions of T and $\vec{\mu}$. One thus may evaluate c_s^2 by either taking numerically the T-derivatives appearing in Eq. (42) or use directly Eqs. (C2)–(C5). The results shown in Fig. 16 are based on the former approach.

As can be seen in Fig. 15 (left) and (middle) the shape of $p(T)$ and $\epsilon(T)$ varies little when changing s/n_B and follows a similar pattern in both quantities. In the temperature range currently accessible to us we thus do not expect to observe a strong dependence of the speed of sound and the adiabatic compressibility on s/n_B. This is indeed apparent from the results for both observables, calculated for several fixed ratios s/n_B, as shown in Fig. 16. At low temperatures we show results for c_s^2 only down to T-values that can be reached at fixed s/n_B for $\hat{\mu}_B < 2.5$. As can be seen in Fig. 14 this allows to explore the entire available temperature range ($T > 135$ MeV) for $s/n_B \geq 30$, but limits the temperature range for smaller values of s/n_B.

At zero baryon density ($s/n_B = \infty$) the speed of sound has a minimum at $T = 145$–150 MeV [5]. From Fig. 16 (left) we see that for temperatures $T > 145$ MeV the speed of sound slightly increases with decreasing s/n_B and steadily increases with T. At temperatures $T < 145$ MeV the opposite trend is expected to show up in HRG model calculations: c_s^2 decreases with decreasing s/n_B and increasing T, see Fig. 16 (left). At low temperatures, the speed of sound is known to have a "bump" arising from the interplay of baryon and light meson contributions to c_s^2. This is apparent from the inset in Fig. 16 (left), where we show results on the speed of sound calculated in a HRG model using the QMHRG2020 list of hadrons for several representative values of s/n_B. The bump in the speed of sound at low temperature is responsible for the minimum in c_s^2 at $T = 145$–150 MeV observed in lattice QCD calculations. This bump, however, will disappear with decreasing s/n_B. The HRG model calculation shown in the inset of 16 (left) indicate that c_s^2 will stop developing a bump at low temperatures at $s/n_B \simeq 15$. Therefore, we expect that the minimum in c_s^2 will become shallower and its position will possibly shift to smaller temperatures with decreasing

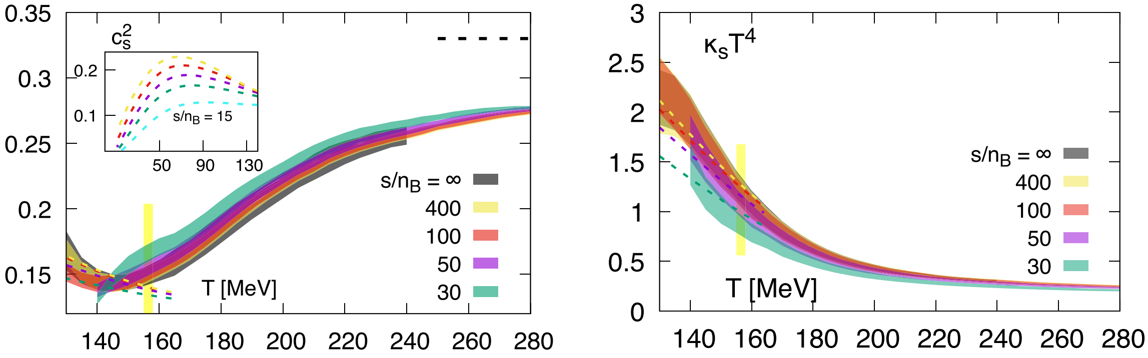

FIG. 16. Speed of sound (left) and adiabatic compressibility (right) in strangeness-neutral, isospin-symmetric matter versus temperature. Shown are results for several values of s/n_B. The limit $s/n_B = \infty$ corresponds to the case of vanishing chemical potentials. Dashed lines at low temperatures indicate QMHRG2020 model calculations, at high temperatures they show the noninteracting quark-gluon gas results. In the inset HRG model calculations at lower temperatures are shown. The yellow band indicates T_{pc}.

s/n_B. Lattice QCD calculations for $s/n_B = 100$ shown in Fig. 16 (left) seem to confirm this expectation. For sufficiently small s/n_B the minimum in the speed of sound may disappear altogether.

As c_s^2 as well as ϵ and p increase with decreasing s/n_B it is clear that the adiabatic compressibility shown in Fig. 16 (right) will decrease with decreasing s/n_B. Moreover we find that it monotonically decreases with increasing temperature.

VI. CONCLUSIONS

We presented an update on the Taylor expansion of basic thermodynamic observable (pressure, energy, and entropy densities) of strangeness-neutral, isospin-symmetric strong-interaction matter. We showed that the $\hat{\mu}_B$-dependent parts of these observables approach the high-temperature perturbative regime much more rapidly than the contribution to these observables at $\hat{\mu}_B = 0$. The $\hat{\mu}_B$-dependent contributions are well described by $\mathcal{O}(g^2)$ perturbation theory already for $T \gtrsim 250$ MeV.

We furthermore constructed the QCD equation of state $[P(n_B), \epsilon(n_B)]$. We showed that the Taylor series can be resummed using Padé approximants. The regime where Taylor expansions and Padé approximants agree with each other gives further confidence in the validity range of current Taylor expansion results varying from $\hat{\mu}_B \simeq 2.5$ at low temperatures to $\hat{\mu}_B \gtrsim 3$ at $T > 200$ MeV.

We showed that $\mathcal{O}(\hat{\mu}_B^4)$ Taylor series results for the pressure provide a good description of the EoS in almost the entire parameter range currently accessible in the beam energy scan performed at RHIC in collider mode. This allows for an analytic ansatz for the $\hat{\mu}_B$-dependent part of the EoS of strangeness-neutral, isospin-symmetric matter, valid at temperatures $T \gtrsim 135$ MeV and $\mu_B/T \lesssim 2.5$, which requires as input only the two leading-order Taylor expansion coefficients $[P_2(T), P_4(T)]$ of the pressure series. We note, however, that this conclusion is based on lattice calculation with $N_\tau = 8$ lattices only.

For the first time, we presented results for the speed of sound in strangeness-neutral matter at nonzero net baryon-number density. We showed that the minimum in c_s^2 becomes shallower and its position shifts toward smaller temperatures for $s/n_B \le 100$. It is possible that this minimum will disappear for sufficiently small s/n_B. All data presented in the figures of this paper can be found in Ref. [48].

ACKNOWLEDGMENTS

This work was supported by: (i) The U.S. Department of Energy, Office of Science, Office of Nuclear Physics through the Contract No. DE-SC0012704; (ii) The U.S. Department of Energy, Office of Science, Office of Nuclear Physics within the framework of Scientific Discovery through Advance Computing (SciDAC) award *Fundamental Nuclear Physics at the Exascale and Beyond*; (iii) The Deutsche Forschungsgemeinschaft (DFG, German Research Foundation)—Project Numbers 315477589-TRR 211 and 460248186 (PUNCH4NFDI); (iv) The Grant No. 05P2018 (ErUM-FSP T01) of the German Bundesministerium für Bildung und Forschung; (v) The Grant No. 283286 of the European Union. D. B. was supported by the Intel Corporation. This research used awards of computer time provided by: (i) The INCITE program at Oak Ridge Leadership Computing Facility, a DOE Office of Science User Facility operated under Contract No. DE-AC05-00OR22725; (ii) The ALCC program at National Energy Research Scientific Computing Center, a U.S. Department of Energy Office of Science User Facility operated under Contract No. DE-AC02-05CH11231; (iii) The INCITE program at Argonne Leadership Computing Facility, a U.S. Department of Energy Office of Science User Facility operated under Contract No. DE-AC02-06CH11357; (iv) The USQCD resources at the Thomas Jefferson National Accelerator Facility. This research also used computing resources made available through: (i) a PRACE grant at CINECA, Italy; (ii) the Gauss Centre for Supercomputing at the Jülich

Supercomputing Centre, Germany; (iii) the GPU-cluster at Bielefeld University, Germany. We thank the Bielefeld HPC.NRW team for their support and Dietrich Boedeker for very helpful discussions.

APPENDIX A: CONSTRAINED PARTIAL DERIVATIVES

We summarize here relations for partial derivatives of thermodynamic observables with respect to temperature, keeping specific external conditions (x, y, z) fixed,

For any thermodynamic function $f(T, \mu_B, \mu_Q, \mu_S)$ we have

$$\left(\frac{\partial f}{\partial T}\right)_{(x,y,z)} = \left(\frac{\partial f}{\partial T}\right)_{(\mu_B,\mu_Q,\mu_S)} + \left(\frac{\partial f}{\partial \mu_B}\right)_{(T,\mu_Q,\mu_S)} \left(\frac{\partial \mu_B}{\partial T}\right)_{(x,y,z)} + \left(\frac{\partial f}{\partial \mu_Q}\right)_{(T,\mu_B,\mu_S)} \left(\frac{\partial \mu_Q}{\partial T}\right)_{(x,y,z)} + \left(\frac{\partial f}{\partial \mu_S}\right)_{(T,\mu_B,\mu_Q)} \left(\frac{\partial \mu_S}{\partial T}\right)_{(x,y,z)}. \tag{A1}$$

Similarly one has for two thermodynamic functions $f(T, \mu_B, \mu_Q, \mu_S)$ and $g(T, \mu_B, \mu_Q, \mu_S)$ the relation

$$\left(\frac{\partial f}{\partial g}\right)_{(x,y,z)} = \frac{(\partial f/\partial T)_{(x,y,z)}}{(\partial g/\partial T)_{(x,y,z)}}. \tag{A2}$$

In Eqs. (A1) and (A2) the derivatives of the chemical potentials are taken on lines of constant $x(T, \mu_B, \mu_Q, \mu_S)$, $y(T, \mu_B, \mu_Q, \mu_S)$, and $z(T, \mu_B, \mu_Q, \mu_S)$ in the space of external parameters (T, μ_B, μ_Q, μ_S). In the lattice QCD context we usually work in the parameter space $(T, \hat{\mu} \equiv \mu/T)$. Moreover, we conveniently work with reduced, i.e., dimensionless, thermodynamic observables, i.e., we want to replace, e.g., $\hat{\epsilon} = \epsilon/T^4$, etc.

Changing the partial derivatives ∂_{μ_B} to $\partial_{\mu_B/T}$ and introducing reduced observables is straightforward, as these derivatives are taken at fixed T. We have for an observable that has dimension of T^n the relation,

$$\left.\frac{\partial f}{\partial \mu_B}\right|_T = T^{n-1} \left.\frac{\partial \hat{f}}{\partial \hat{\mu}_B}\right|_T. \tag{A3}$$

Rewriting the temperature derivatives one has to be a bit more careful,

$$\begin{aligned} \left.\frac{\partial f}{\partial T}\right|_{\vec{\mu}} &= \left.\frac{\partial f}{\partial T}\right|_{\vec{\hat{\mu}}} - \sum_{i=B,Q,S} \frac{\mu_i}{T^2} \left.\frac{\partial f}{\partial \mu_i/T}\right|_T \\ &= \left.\frac{\partial T^n \hat{f}}{\partial T}\right|_{\vec{\hat{\mu}}} - \sum_i \frac{\mu_i}{T^2} T^n \left.\frac{\partial \hat{f}}{\partial \hat{\mu}_i}\right|_T \\ &= T^{n-1}\left(n\hat{f} + T\left.\frac{\partial \hat{f}}{\partial T}\right|_{\vec{\hat{\mu}}} - \sum_i \hat{\mu}_i \left.\frac{\partial \hat{f}}{\partial \hat{\mu}_i}\right|_T\right). \end{aligned} \tag{A4}$$

APPENDIX B: IDEAL GAS AND HIGH-TEMPERATURE PERTURBATION THEORY FOR ISOSPIN-SYMMETRIC, STRANGENESS-NEUTRAL MATTER

At large values of the temperature, the pressure approaches that of a massless ideal gas of quarks and gluons. In the case of massless quarks, the leading order, ideal gas result as well as the $\mathcal{O}(g^2)$ correction are second-order polynomials in $\hat{\mu}_f^2$ [49,50],

$$p/T^4 = \hat{p}_{id} - g^2 \hat{p}_2, \tag{B1}$$

with the ideal gas term

$$\hat{p}_{id} = \frac{8\pi^2}{45}\left(1 + \frac{21 n_f}{32}\right) + \sum_{f=u,d,s}\left[\frac{1}{2}\left(\frac{\mu_f}{T}\right)^2 + \frac{1}{4\pi^2}\left(\frac{\mu_f}{T}\right)^4\right], \tag{B2}$$

and the $\mathcal{O}(g^2)$ correction

$$\hat{p}_2 = \frac{1}{6}\left(1 + \frac{5 n_f}{12}\right) + \frac{1}{2\pi^2}\sum_{f=u,d,s}\left[\frac{1}{2}\left(\frac{\mu_f}{T}\right)^2 + \frac{1}{4\pi^2}\left(\frac{\mu_f}{T}\right)^4\right], \tag{B3}$$

Expressing the flavor chemical potentials in terms of conserved charge chemical potentials,

$$\begin{aligned} \hat{\mu}_u &= (\hat{\mu}_B + 2\hat{\mu}_Q)/3, \\ \hat{\mu}_d &= (\hat{\mu}_B - \hat{\mu}_Q)/3, \\ \hat{\mu}_s &= (\hat{\mu}_B - \hat{\mu}_Q)/3 - \hat{\mu}_S, \end{aligned} \tag{B4}$$

the strangeness number density can be written as

$$\hat{n}_S = -\frac{1 - q_1 - 3s_1}{3}\left(1 + \frac{1}{2\pi^2} g^2\right) \times \left(\hat{\mu}_B + -\frac{(1 - q_1 - 3s_1)^2}{18\pi^2}\hat{\mu}_B^3\right) \tag{B5}$$

Here we introduced the ratio of chemical potentials, $s_1 = \hat{\mu}_S/\hat{\mu}_B$ and $q_1 = \hat{\mu}_Q/\hat{\mu}_B$. From Eq. (B5) we find the constraint for a strangeness-neutral ideal gas,

$$s_1 = \frac{1 - q_1}{3}. \tag{B6}$$

Inserting this constraint in Eq. (B4) one finds that up to $\mathcal{O}(g^2)$ in perturbation theory the strange quark chemical potential vanishes in strangeness-neutral matter, $\mu_s = 0$. Moreover, the electric charge chemical potential vanishes ($\mu_Q = 0$) in the isospin-symmetric case $n_u = n_d$. Up to $\mathcal{O}(g^2)$ we thus may write for the $\hat{\mu}_B$-dependent contribution

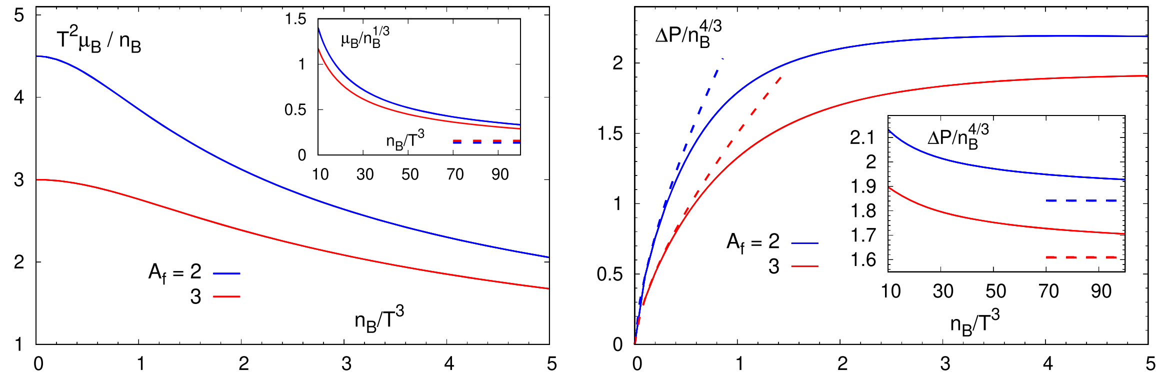

FIG. 17. Baryon chemical potential (left) and the μ_B-dependent part of the pressure (right) of a 3-flavor, ideal gas of massless quarks versus net baryon-number density (n_B). Shown are results for the cases ($\mu_Q = 0, n_S = 0$) ($A_f = 2$) and ($\mu_Q = 0, \mu_S = 0$) ($A_f = 3$). Results are rescaled with powers of n_B appropriate in the low density (main panel) and high density (insets) limits, respectively. Dashed lines show the respective low and high density limits.

to the pressure of an isospin-symmetric medium and the two cases[9] of interest to us (i) $\mu_S = 0$ or (ii) $n_S = 0$,

$$\Delta p/T^4 = \frac{A_f}{18}\left(1 - \frac{g^2}{2\pi^2}\right)\left(\hat{\mu}_B^2 + \frac{1}{18\pi^2}\hat{\mu}_B^4\right), \tag{B7}$$

$$n_B/T^3 = \frac{A_f}{9}\left(1 - \frac{g^2}{2\pi^2}\right)\left(\hat{\mu}_B + \frac{1}{9\pi^2}\hat{\mu}_B^3\right), \tag{B8}$$

where $A_f = 3$ for $\mu_S = 0$ and $A_f = 2$ for $n_S = 0$.

For the coupling g^2 we use the two-loop running coupling, allowing for a free parameter in the renormalization scale, $k_T\pi T$, as it also is used in more refined, resummed approaches, e.g., hard thermal loop (HTL) calculations [30],

$$\begin{aligned} \beta_0 &= \frac{11 - 2n_f/3}{4\pi} \\ \beta_1 &= \frac{102 - 38n_f/3}{16\pi^2} \\ g_{1\text{loop}}^2 &= \frac{2\pi}{\beta_0 \ln\left(k_T\pi T/\Lambda_{\overline{\text{MS}}}\right)}, \end{aligned} \tag{B9}$$

$$g^2 = g_{1\text{loop}}^2\left[1 - \frac{\beta_1}{\beta_0^2}\frac{\ln(2\ln(k_T\pi T/\Lambda_{\overline{\text{MS}}}))}{2\ln(k_T\pi T/\Lambda_{\overline{\text{MS}}})}\right], \tag{B10}$$

with $n_f = 3$. As a scale factor we use the average of recent values summarized in the last FLAG report $\Lambda_{\overline{\text{MS}}} = 339(12)$ MeV [51].

From Eqs. (B7) and (B8) we easily find the low and high density limits of the EoS of a massless, strangeness-neutral, isospin-symmetric quark gas to $\mathcal{O}(g^2)$ in high-T perturbation theory,

$$\frac{\Delta p}{T^4} = \begin{cases} \frac{9}{2A_f(1-g^2/2\pi^2)}\left(\frac{n_B}{T^3}\right)^2, & \frac{n_B}{T^3} \ll 1, \\ \frac{1}{4}\left(\frac{81\pi^2}{A_f(1-g^2/2\pi^2)}\right)^{1/3}\left(\frac{n_B}{T^3}\right)^{4/3}, & \frac{n_B}{T^3} \gg 1. \end{cases} \tag{B11}$$

For arbitrary net baryon-number densities we invert Eq. (B8) to obtain the baryon chemical potential as function of n_B/T^3 in $\mathcal{O}(g^2)$ perturbation theory,

$$\hat{\mu}_B(\hat{n}_B) = y^{1/3} - \frac{3\pi^2}{y^{1/3}}, \tag{B12}$$

with

$$y = \frac{3^4\pi^2}{2A_f(1 - g^2/2\pi^2)} \times\left(\hat{n}_B + \sqrt{\hat{n}_B^2 + (2\pi A_f(1 - g^2/2\pi^2))^2/3^5}\right). \tag{B13}$$

Inserting Eq. (B12) in Eq. (B7) we obtain the equation of state of strangeness-neutral, isospin-symmetric matter in the high-temperature limit. The result in the ideal gas limit ($g^2 = 0$) is shown in Fig. 17. Comparing with Fig. 4 one sees that the density range covered at high temperature in current Taylor series expansions with $\hat{\mu}_B \le 2.5$, i.e., $n_B/T^3 < 0.6$ corresponds to the low density limit of an ideal gas, $\mu_B/T \sim n_B/T^3$. The transition between the low and high density regions, however, starts to set in for $n_B/T^3 \gtrsim 0.6$.

---

[9] Because of isospin symmetry and strangeness-neutrality conditions that we impose, one has $\mu_s = 0$ at high temperature. For this reason, strange quarks do not contribute to the density dependent part, in particular the net baryon-number density of the ideal gas and LO perturbative limits. This is reflected in the parameter A_f.

APPENDIX C: SPEED OF SOUND

The speed of sound is defined as

$$c^2_{\vec{X}} = \left(\frac{\partial p}{\partial \epsilon}\right)_{\vec{X}}, \tag{C1}$$

where $\vec{X}$ defines the external conditions, e.g., constant entropy per particle number. We generalize this here to the case of QCD, where three conserved currents need to be specified. We do so by choosing $\vec{X} = (s/n_B, n_Q/n_B, n_S)$ With this we obtain

$$c^2_{\vec{X}} = \frac{N_{\vec{X}}}{(\epsilon + p - \mu_S n_S) D_{\vec{X}}}, \tag{C2}$$

with

$$\begin{aligned} N_{\vec{X}} &= s^2 a_{s2} + s' a_s + s(s_B a_B + s_Q a_Q + s_S a_S) + s_B^2 a_{B2} + s_Q^2 a_{Q2} + s_S^2 a_{S2} + s_B s_Q a_{BQ} + s_B s_S a_{BS} + s_Q s_S a_{QS} \\ D_{\vec{X}} &= s' b_s + s_B^2 b_{B2} + s_Q^2 b_{Q2} + s_S^2 b_{S2} + s_B s_Q b_{BQ} + s_B s_S b_{BS} + s_Q s_S b_{QS} \end{aligned} \tag{C3}$$

Here we use the abbreviation s_i for the derivatives of the entropy with respect to the chemical potential μ_i, i.e., $s_i = \partial s/\partial \mu_i$.

Using $n_Q/n_B = r$, the various coefficients appearing in Eq. (C3) are given by

$$\begin{aligned} a_{s2} &= -(\chi_{11}^{BS})^2 \chi_2^Q + 2\chi_{11}^{BQ}\chi_{11}^{BS}\chi_{11}^{QS} - \chi_2^B(\chi_{11}^{QS})^2 - (\chi_{11}^{BQ})^2\chi_2^S + \chi_2^B\chi_2^Q\chi_2^S \\ a_s &= -(r^2 b_{Q2} + r b_{BQ} + b_{B2}) n_B^2 - \frac{1}{2}(r b_{QS} + b_{BS}) n_B n_S \\ a_B &= (2b_{B2} + r b_{BQ}) n_B + \frac{1}{2} b_{BS} n_S \\ a_Q &= (b_{BQ} + 2r b_{Q2}) n_B + \frac{1}{2} b_{QS} n_S \\ a_S &= (b_{BS} + r b_{QS}) n_B + b_{S2} n_S \\ a_{B2} &= -r^2 \chi_2^S n_B^2 + r\chi_{11}^{QS} n_B n_S \\ a_{Q2} &= -\chi_2^S n_B^2 + \chi_{11}^{BS} n_B n_S \\ a_{S2} &= (2r\chi_{11}^{BQ} - r^2\chi_2^B - \chi_2^Q) n_B^2 \\ a_{BQ} &= 2r\chi_2^S n_B^2 - (r\chi_{11}^{BS} + \chi_{11}^{QS}) n_B n_S \\ a_{BS} &= -2r(\chi_{11}^{QS} - r\chi_{11}^{BS}) n_B^2 + (\chi_2^Q - r\chi_{11}^{BQ}) n_B n_S \\ a_{QS} &= 2(\chi_{11}^{QS} - r\chi_{11}^{BS}) n_B^2 + (r\chi_2^B - \chi_{11}^{BQ}) n_B n_S \end{aligned} \tag{C4}$$

$$\begin{aligned} b_s &= a_{s2} \\ b_{B2} &= (\chi_{11}^{QS})^2 - \chi_2^Q\chi_2^S \\ b_{Q2} &= (\chi_{11}^{BS})^2 - \chi_2^B\chi_2^S \\ b_{S2} &= (\chi_{11}^{BQ})^2 - \chi_2^B\chi_2^Q \\ b_{BQ} &= 2(\chi_{11}^{BQ}\chi_2^S - \chi_{11}^{BS}\chi_{11}^{QS}) \\ b_{BS} &= 2(\chi_{11}^{BS}\chi_2^Q - \chi_{11}^{BQ}\chi_{11}^{QS}) \\ b_{QS} &= 2(\chi_{11}^{QS}\chi_2^B - \chi_{11}^{BQ}\chi_{11}^{BS}) \end{aligned} \tag{C5}$$

We note that all cumulants χ_{11}^{ab} and χ_2^c, with $a, b = B, Q, S$, appearing in Eqs. (C4) and (C5) are defined as μ_i, $i = a, b$, derivatives of P and as such are functions of the chemical potentials, i.e., $\chi_{11}^{ab} \equiv \chi_{11}^{ab}(\mu_B, \mu_Q, \mu_S)$. They need to be chosen such that the constraint $\vec{X}$ is satisfied.

For $\vec{\mu} = 0$ Eq. (C3) reduces to $N_{\vec{\mu}=0} = s^2 a_{s2}$ and $D_{\vec{\mu}=0} = s' b_s$. All other coefficients appearing in Eqs. (C4) and (C5) are proportional to μ^2.

As discussed in Appendix A some care has to be taken when rewriting the derivatives of, e.g., entropy density with respect to T,

$$s' \equiv \left.\frac{\partial s}{\partial T}\right|_{\vec{\mu}} = T^2\left(3\hat{s} + T\left.\frac{\partial \hat{s}}{\partial T}\right|_{\hat{\vec{\mu}}} - \sum_i \hat{\mu}_i \left.\frac{\partial \hat{s}}{\partial \hat{\mu}_i}\right|_T\right). \tag{C6}$$

For $\vec{\mu} = 0$ we obtain the well-known expression

$$c_s^2|_{\vec{\mu}=0} = \frac{s}{Ts'}\bigg|_{\vec{\mu}=0}. \tag{C7}$$

Furthermore, for an ideal gas Eq. (C2) gives, of course, $c_s^2 = 1/3$ for arbitrary (μ_B, μ_Q, μ_S).

We are interested here in the speed of sound in strangeness-neutral matter. In that case all terms proportional to n_S appearing in Eqs. (C2) and (C4) can be set to zero.

[1] P. Braun-Munzinger, V. Koch, T. Schäfer, and J. Stachel, Properties of hot and dense matter from relativistic heavy ion collisions, Phys. Rep. **621**, 76 (2016).

[2] M. M. Middeldorf-Wygas, I. M. Oldengott, D. Bödeker, and D. J. Schwarz, Cosmic QCD transition for large lepton flavor asymmetries, Phys. Rev. D **105**, 123533 (2022).

[3] F. Karsch, E. Laermann, and A. Peikert, The pressure in two flavor, (2 + 1)-flavor and three flavor QCD, Phys. Lett. B **478**, 447 (2000).

[4] S. Borsanyi, Z. Fodor, C. Hoelbling, S. D. Katz, S. Krieg, and K. K. Szabo, Full result for the QCD equation of state with 2 + 1 flavors, Phys. Lett. B **730**, 99 (2014).

[5] A. Bazavov *et al.* (HotQCD Collaboration), Equation of state in (2 + 1)-flavor QCD, Phys. Rev. D **90**, 094503 (2014).

[6] R. V. Gavai and S. Gupta, Quark number susceptibilities, strangeness and dynamical confinement, Phys. Rev. D **64**, 074506 (2001).

[7] C. R. Allton, S. Ejiri, S. J. Hands, O. Kaczmarek, F. Karsch, E. Laermann, C. Schmidt, and L. Scorzato, The QCD thermal phase transition in the presence of a small chemical potential, Phys. Rev. D **66**, 074507 (2002).

[8] M. D'Elia and M.-P. Lombardo, Finite density QCD via imaginary chemical potential, Phys. Rev. D **67**, 014505 (2003).

[9] P. de Forcrand and O. Philipsen, The QCD phase diagram for small densities from imaginary chemical potential, Nucl. Phys. **B642**, 290 (2002).

[10] S. Borsanyi, G. Endrodi, Z. Fodor, S. D. Katz, S. Krieg, C. Ratti, and K. K. Szabo, QCD equation of state at nonzero chemical potential: Continuum results with physical quark masses at order μ^2, J. High Energy Phys. 08 (2012) 053.

[11] J. N. Guenther, R. Bellwied, S. Borsanyi, Z. Fodor, S. D. Katz, A. Pasztor, C. Ratti, and K. K. Szabó, The QCD equation of state at finite density from analytical continuation, Nucl. Phys. **A967**, 720 (2017).

[12] S. Borsanyi, J. N. Guenther, R. Kara, Z. Fodor, P. Parotto, A. Pasztor, C. Ratti, and K. K. Szabo, Resummed lattice QCD equation of state at finite baryon density: Strangeness neutrality and beyond, Phys. Rev. D **105**, 114504 (2022).

[13] S. Ejiri, F. Karsch, E. Laermann, and C. Schmidt, The isentropic equation of state of 2-flavor QCD, Phys. Rev. D **73**, 054506 (2006).

[14] A. Bazavov *et al.*, The QCD equation of state to $\mathcal{O}(\mu_B^6)$ from lattice QCD, Phys. Rev. D **95**, 054504 (2017).

[15] D. Bollweg, J. Goswami, O. Kaczmarek, F. Karsch, S. Mukherjee, P. Petreczky, C. Schmidt, and P. Scior (HotQCD Collaboration), Taylor expansions and Padé approximants for cumulants of conserved charge fluctuations at nonvanishing chemical potentials, Phys. Rev. D **105**, 074511 (2022).

[16] R. V. Gavai, S. Gupta, and S. Mukherjee, The speed of sound and specific heat in the QCD plasma: Hydrodynamics, fluctuations and conformal symmetry, Phys. Rev. D **71**, 074013 (2005).

[17] S. Floerchinger and M. Martinez, Fluid dynamic propagation of initial baryon number perturbations on a Bjorken flow background, Phys. Rev. C **92**, 064906 (2015).

[18] A. Bazavov *et al.*, Skewness, kurtosis, and the fifth and sixth order cumulants of net baryon-number distributions from lattice QCD confront high-statistics STAR data, Phys. Rev. D **101**, 074502 (2020).

[19] P. Dimopoulos, L. Dini, F. Di Renzo, J. Goswami, G. Nicotra, C. Schmidt, S. Singh, K. Zambello, and F. Ziesché, Contribution to understanding the phase structure of strong interaction matter: Lee-Yang edge singularities from lattice QCD, Phys. Rev. D **105**, 034513 (2022).

[20] L. Mazur, Topological aspects in lattice QCD, Ph.D. thesis, Bielefeld University, 2021.

[21] D. Bollweg, L. Altenkort, D. A. Clarke, O. Kaczmarek, L. Mazur, C. Schmidt, P. Scior, and H.-T. Shu, HotQCD on multi-GPU systems, Proc. Sci. LATTICE2021 (**2022**) 196 [arXiv:2111.10354].

[22] L. Mazur *et al.*, SIMULATeQCD: A simple multi-GPU lattice code for QCD calculations, arXiv:2306.01098.

[23] D. Bollweg, J. Goswami, O. Kaczmarek, F. Karsch, S. Mukherjee, P. Petreczky, C. Schmidt, and P. Scior (HotQCD Collaboration), Second order cumulants of conserved charge fluctuations revisited: Vanishing chemical potentials, Phys. Rev. D **104**, 074512 (2021).

[24] `AnalysisToolbox`: A set of Python tools for analyzing physics data, in particular targeting lattice QCD, https://github.com/LatticeQCD/AnalysisToolbox.

[25] P. Virtanen *et al.*, SciPy 1.0: Fundamental algorithms for scientific computing in Python, Nat. Methods **17**, 261 (2020).

[26] M. D'Elia, G. Gagliardi, and F. Sanfilippo, Higher order quark number fluctuations via imaginary chemical potentials in $N_f = 2 + 1$ QCD, Phys. Rev. D **95**, 094503 (2017).

[27] S. Borsanyi, Z. Fodor, J. N. Guenther, S. K. Katz, K. K. Szabo, A. Pasztor, I. Portillo, and C. Ratti, Higher order fluctuations and correlations of conserved charges from lattice QCD, J. High Energy Phys. 10 (2018) 205.

[28] A. Bazavov *et al.* (HotQCD Collaboration), Chiral crossover in QCD at zero and nonzero chemical potentials, Phys. Lett. B **795**, 15 (2019).

[29] N. Haque, A. Bandyopadhyay, J. O. Andersen, M. G. Mustafa, M. Strickland, and N. Su, Three-loop HTLpt thermodynamics at finite temperature and chemical potential, J. High Energy Phys. 05 (2014) 027.

[30] S. Mogliacci, J. O. Andersen, M. Strickland, N. Su, and A. Vuorinen, Equation of state of hot and dense QCD: Resummed perturbation theory confronts lattice data, J. High Energy Phys. 12 (2013) 055.

[31] A. Bazavov, H. T. Ding, P. Hegde, F. Karsch, C. Miao, S. Mukherjee, P. Petreczky, C. Schmidt, and A. Velytsky, Quark number susceptibilities at high temperatures, Phys. Rev. D **88**, 094021 (2013).

[32] H. T. Ding, S. Mukherjee, H. Ohno, P. Petreczky, and H. P. Schadler, Diagonal and off-diagonal quark number susceptibilities at high temperatures, Phys. Rev. D **92**, 074043 (2015).

[33] R. Bellwied, S. Borsanyi, Z. Fodor, S. D. Katz, A. Pasztor, C. Ratti, and K. K. Szabo, Fluctuations and correlations in high temperature QCD, Phys. Rev. D **92**, 114505 (2015).

[34] G. M. Prosperi, M. Raciti, and C. Simolo, On the running coupling constant in QCD, Prog. Part. Nucl. Phys. **58**, 387 (2007).

[35] D. A. Clarke, O. Kaczmarek, F. Karsch, A. Lahiri, and M. Sarkar, Sensitivity of the Polyakov loop and related observables to chiral symmetry restoration, Phys. Rev. D **103**, L011501 (2021).

[36] S. Borsanyi, Z. Fodor, J. N. Guenther, R. Kara, S. D. Katz, P. Parotto, A. Pasztor, C. Ratti, and K. K. Szabo, QCD Crossover at Finite Chemical Potential from Lattice Simulations, Phys. Rev. Lett. **125**, 052001 (2020).

[37] A. Y. Kotov, M. P. Lombardo, and A. Trunin, QCD transition at the physical point, and its scaling window from twisted mass Wilson fermions, Phys. Lett. B **823**, 136749 (2021).

[38] A. Pelissetto and E. Vicari, Relevance of the axial anomaly at the finite-temperature chiral transition in QCD, Phys. Rev. D **88**, 105018 (2013).

[39] O. Kaczmarek, F. Karsch, E. Laermann, C. Miao, S. Mukherjee, P. Petreczky, C. Schmidt, W. Soeldner, and W. Unger, Phase boundary for the chiral transition in $(2+1)$-flavor QCD at small values of the chemical potential, Phys. Rev. D **83**, 014504 (2011).

[40] F. Karsch, Critical behavior and net-charge fluctuations from lattice QCD, Proc. Sci. CORFU2018 (**2019**) 163 [arXiv:1905.03936].

[41] R. Bellwied, S. Borsanyi, Z. Fodor, J. Günther, S. D. Katz, C. Ratti, and K. K. Szabo, The QCD phase diagram from analytic continuation, Phys. Lett. B **751**, 559 (2015).

[42] C. Bonati, M. D'Elia, F. Negro, F. Sanfilippo, and K. Zambello, Curvature of the pseudocritical line in QCD: Taylor expansion matches analytic continuation, Phys. Rev. D **98**, 054510 (2018).

[43] S. Mukherjee and V. Skokov, Universality driven analytic structure of the QCD crossover: Radius of convergence in the baryon chemical potential, Phys. Rev. D **103**, L071501 (2021).

[44] M. Giordano and A. Pásztor, Reliable estimation of the radius of convergence in finite density QCD, Phys. Rev. D **99**, 114510 (2019).

[45] M. Giordano, K. Kapas, S. D. Katz, D. Nogradi, and A. Pasztor, Radius of convergence in lattice QCD at finite μ_B with rooted staggered fermions, Phys. Rev. D **101**, 074511 (2020); **104**, 119901(E) (2021).

[46] L. Adamczyk *et al.* (STAR Collaboration), Bulk properties of the medium produced in relativistic heavy-ion collisions from the beam energy scan program, Phys. Rev. C **96**, 044904 (2017).

[47] M. D'Elia, High-temperature QCD: Theory overview, Nucl. Phys. **A982**, 99 (2019).

[48] D. Bollweg, D. A. Clarke, J. Goswami, O. Kaczmarek, F. Karsch, S. Mukherjee, P. Petreczky, C. Schmidt, and S. Sharma, Dataset for "Equation of state and speed of sound of $(2+1)$-flavor QCD in strangeness-neutral matter at non-vanishing net baryon-number density" (2023), 10.4119/unibi/2980715.

[49] E. V. Shuryak, Theory of hadronic plasma, Sov. Phys. JETP **47**, 212 (1978).

[50] S. A. Chin, Transition to hot quark matter in relativistic heavy-ion collision, Phys. Lett. **78B**, 552 (1978).

[51] Y. Aoki *et al.* (Flavour Lattice Averaging Group (FLAG)), FLAG review 2021, Eur. Phys. J. C **82**, 869 (2022).